

# Kinetics of Phase Separation in Thin Films: Simulations for the Diffusive Case

Subir K. Das<sup>1</sup>, Sanjay Puri<sup>2</sup>, Jürgen Horbach<sup>1</sup> and K. Binder<sup>1</sup>

<sup>1</sup>*Institut für Physik, Johannes Gutenberg-Universität*

*D-55099 Mainz, Staudinger Weg 7, Germany*

<sup>2</sup>*School of Physical Sciences, Jawaharlal*

*Nehru University, New Delhi-110067, India*

## Abstract

We study the diffusion-driven kinetics of phase separation of a symmetric binary mixture (AB), confined in a thin-film geometry between two parallel walls. We consider cases where (a) both walls preferentially attract the same component (A), and (b) one wall attracts A and the other wall attracts B (with the same strength). We focus on the interplay of phase separation and wetting at the walls, which is referred to as *surface-directed spinodal decomposition* (SDSD). The formation of SDSD waves at the two surfaces, with wave-vectors oriented perpendicular to them, often results in a metastable layered state (also referred to as “stratified morphology”). This state is reminiscent of the situation where the thin film is still in the one-phase region but the surfaces are completely wet, and hence coated with thick wetting layers. This metastable state decays by spinodal fluctuations and crosses over to an asymptotic growth regime characterized by the lateral coarsening of pancake-like domains. These pancakes may or may not be coated by precursors of wetting layers. We use Langevin simulations to study this crossover and the growth kinetics in the asymptotic coarsening regime.

## I. INTRODUCTION

Consider a binary mixture (AB) with a miscibility gap, such that phase separation into A-rich and B-rich phases occurs below the critical temperature  $T_c$ . If this mixture is quenched from a homogeneous state in the one-phase region into the two-phase region below the critical point, phase separation proceeds by the emergence and growth of regions enriched in either component. In the bulk, this process of *spinodal decomposition* or *domain growth* has been intensively studied [1, 2, 3, 4, 5].

In recent years, the effect of surfaces on this behavior has become a focus of research [6, 7, 8, 9, 10, 11, 12, 13]. It is often the case that a surface (S) has a preferential attraction for one of the components (say, A) of the mixture. In the one-phase region of the mixture, this attraction leads to the formation of surface enrichment layers of the preferred component. The thickness of these layers (which is comparable to the correlation length  $\xi_b$  of concentration fluctuations in the bulk) becomes long-ranged at the critical point of the mixture [14, 15]. In addition, if the composition of the bulk mixture coincides with the B-rich branch of the coexistence curve describing phase separation in equilibrium, the surface is coated with an A-rich wetting layer for temperatures below the wetting transition temperature  $T_w$  [16, 17, 18, 19, 20, 21, 22]. Of course, wetting layers of mesoscopic thickness (in the idealized case, the thickness of the wetting layer diverges when complete wetting occurs [19, 20, 21, 22]) can only occur in macroscopic systems. Typically, theoretical approaches consider the idealized case of a semi-infinite geometry [14, 15, 16, 17, 18, 19, 20, 21].

In a thin film of thickness  $D$ , finite-size effects significantly constrain the growth of wetting layers, e.g., for short-range forces between the walls and the A-atoms, the equilibrium thickness of a wetting layer is  $O(\ln D)$  [22, 23, 24, 25]. Further, in a thin-film geometry, the interplay between surface effects and bulk phase separation leads to a distortion of the phase diagram describing lateral phase separation parallel to the walls, analogous to the phenomenon of capillary condensation [22, 24, 25, 26, 27, 28, 29]. Moreover, the critical behavior changes its character from three-dimensional

to two-dimensional [30]. The interplay of wetting and phase separation in a thin film results in a rich phase behavior, and the equilibrium phase diagrams of thin films have been investigated for a range of possible surface forces [22, 29, 31, 32, 33, 34, 35, 36]. In the low-temperature region, relevant for deep quenches to a temperature  $T < T_w$ , the typical state in a thin film with symmetric walls (i.e., both attract A with the same strength) is a laterally-segregated state with a B-rich pancake-like domain. This domain is circular with a macroscopic radius  $R$ , which is of the same order as the macroscopic linear dimension  $L$  parallel to the walls – see Fig. 1(a). For a volume fraction  $\phi_B$  of B-atoms lying between the two branches of the coexistence curve  $\phi_{B,\text{coex}}^{(1)}(D)$ ,  $\phi_{B,\text{coex}}^{(2)}(D)$  of the thin film, the lever rule requires

$$\phi_B = (1 - x)\phi_{B,\text{coex}}^{(1)}(D) + x\phi_{B,\text{coex}}^{(2)}(D) \quad , \quad (1)$$

where  $x$  is the volume fraction of the B-rich phase. For a film of volume  $L^2D$  (Fig. 1) with periodic boundary conditions in the directions parallel to the walls, we have  $x = \pi R^2/L^2$ . Assuming a strongly segregated state where  $\phi_{B,\text{coex}}^{(1)}(D) \simeq 0$ ,  $\phi_{B,\text{coex}}^{(2)}(D) \simeq 1$ , we obtain  $R \simeq L\sqrt{\phi_B/\pi}$  for the radius of the B-rich domain.

In this simple argument, we have assumed that the pancake is cylindrical and its surface is perpendicular to the walls. In fact, the interface is curved because (in the  $D \rightarrow \infty$  limit) the A-B interface meets the wall at a contact angle  $\theta$ , given by Young's equation [37]:

$$\sigma \cos \theta = \gamma_B - \gamma_A \quad . \quad (2)$$

Here,  $\sigma$  is the interfacial tension between the A-rich and B-rich phases; and  $\gamma_A$ ,  $\gamma_B$  are the surface tensions between the A-rich and B-rich phases and the wall, respectively. The surface is partially wet (PW) when  $\sigma > \gamma_B - \gamma_A$  [16, 17, 18, 19, 20, 21, 22]. When  $T \rightarrow T_w^-$ ,  $\theta \rightarrow 0$ , and for  $T > T_w$  one has  $\sigma < \gamma_B - \gamma_A$ . In this complete wetting (CW) situation shown in Fig. 1(b), there is no direct contact between the B-rich phase and the wall – the B-rich pancake is encapsulated by A-rich wetting layers for  $D \rightarrow \infty$ . (For finite  $D$ , only precursors of wetting layers are possible.) The cross-sections of these states [Figs. 1(a)-(b)] are reminiscent of the states considered by Liu et al. [38] in the context of phase separation in cylindrical

pores. Liu et al. made a distinction between elongated plugs in the PW case and capsules in the CW case, respectively. Note, however, that the lateral size of these domains in equilibrium for small  $D$  and  $L \rightarrow \infty$  does not diverge with  $L$ , unlike the present  $d = 2$  cases. Rather the lateral size  $\ell \sim \exp[\sigma\pi D^2/(4k_B T)]$ , where  $D$  is the pore diameter. We also note that, in the CW case the thickness of the B-rich domain differs from  $D$  only by a small amount, that will be estimated below.

It is also interesting to consider equilibrium morphologies in antisymmetric films, i.e., one wall attracts A and the other attracts B with equal strength. In Fig. 1(c), we show a schematic of the PW state in an antisymmetric film. This state also resembles a pancake, except that the cross-section is trapezoidal in this case due to the difference in contact angles at the two walls. In Fig. 1(d), we show a schematic of the CW state in an antisymmetric film. In this state, there is a single A-B interface which is parallel to the walls.

In this paper, we are interested in the kinetic processes which lead to the formation of these structures subsequent to a deep quench from the high-temperature disordered state. In these *surface-directed spinodal decomposition* (SDSD) processes, one typically observes first the formation of a layered structure, consisting of an A-rich layer followed by a depletion layer in A, etc. This layered profile propagates into the bulk, but at a later stage it may break up into a laterally inhomogeneous structure. The kinetics of such growth phenomena has important technological applications, including the fabrication of nanoscale patterns and layered structures. However, despite much effort (for reviews, see [9, 10, 11, 12, 13]) these phenomena are still incompletely understood.

In the present paper, we will study the dynamics of these structure-formation processes for the case where hydrodynamic effects can be disregarded, so that the kinetics is purely diffusive. Therefore, our results will be applicable to solid mixtures, and the early stages of phase separation in polymer and fluid mixtures. (In a subsequent paper, we will elucidate the role of hydrodynamic effects in these problems.) We shall consider the cases of both symmetric and antisymmetric films. This paper is organized as follows: In Sec. II, we describe our dynamical model for segregation

in confined geometries. In Sec. III, we focus on the kinetics of phase separation in a symmetric film, while Sec. IV studies segregation kinetics in an antisymmetric film. We conclude this paper with a summary and discussion in Sec. V.

## II. DYNAMICAL MODEL FOR SEGREGATION IN FILMS

The model for phase separation at surfaces has been developed previously by Puri and Binder [7]. In dimensionless units [10, 13], the free energy functional for an unstable binary mixture in a film extending from  $z = 0$  to  $z = D$  is [39]

$$\begin{aligned}
F[\psi] \simeq & \int d\vec{r} \left[ -\frac{\psi^2}{2} + \frac{\psi^4}{4} + \frac{1}{4}(\vec{\nabla}\psi)^2 + V(z)\psi \right] + \\
& \int_{S_1} d\vec{\rho} \left\{ -\frac{g}{2}[\psi(\vec{\rho}, 0)]^2 - h_1\psi(\vec{\rho}, 0) - \gamma\psi(\vec{\rho}, 0)\frac{\partial\psi}{\partial z}\Big|_{z=0} \right\} + \\
& \int_{S_2} d\vec{\rho} \left\{ -\frac{g}{2}[\psi(\vec{\rho}, D)]^2 - h_2\psi(\vec{\rho}, D) + \gamma\psi(\vec{\rho}, D)\frac{\partial\psi}{\partial z}\Big|_{z=D} \right\} \\
\equiv & F_b + F_{S_1} + F_{S_2} \quad . \tag{3}
\end{aligned}$$

Here,  $\psi(\vec{r})$  is the order parameter which is proportional to the density difference between the two species,  $\psi(\vec{r}) \propto \rho_A(\vec{r}) - \rho_B(\vec{r})$ . It is normalized such that the coexisting A-rich and B-rich bulk phases for  $T < T_c$  correspond to  $\psi = \pm 1$ , respectively. The first term on the RHS of Eq. (3) is the bulk free energy  $F_b$ , with  $V(z)$  being the  $z$ -dependent potential due to the surfaces  $S_1$  and  $S_2$ . In our subsequent discussion, we will consider power-law potentials:  $V(z) = -V_0[(z+1)^{-n} \pm (D+1-z)^{-n}]$ , where the  $+$  and  $-$  signs denote symmetric and antisymmetric films, respectively. Such potentials are common in the context of surface-molecule interactions, e.g.,  $n = \kappa - d$  with  $\kappa = 6$  and  $7$  corresponds to cases with non-retarded and retarded van der Waals' interactions, respectively [40]. The potentials are taken to originate behind the surfaces so as to avoid singularities at  $z = 0, D$ .

The second term  $F_{S_1}$  on the RHS of Eq. (3) is the local contribution from the surface  $S_1$  located at  $z = 0$ . We have written  $\vec{r} = (\vec{\rho}, z)$ , where  $\vec{\rho}$  denotes the  $(d-1)$  coordinates parallel to the surface, and  $z$  denotes the coordinate perpendicular to

the surface. In  $F_{S_1}$ ,  $g$  and  $\gamma$  are parameters which depend on temperature and the exchange couplings in the bulk ( $J$ ) and at the surface ( $J_s$ ) [10, 13]:

$$g = \frac{(q-2)J_s + J - k_B T}{k_B(T_c - T)}, \quad (4)$$

$$\gamma = \frac{J}{2\xi_b k_B(T_c - T)}, \quad \xi_b = \left[ \frac{q}{2} \left( 1 - \frac{T}{T_c} \right) \right]^{-1/2}. \quad (5)$$

Here,  $q$  denotes the coordination number of a site, and  $\xi_b$  is the bulk correlation length. [Our normalization of  $F[\psi]$  in Eq. (3) implies that all lengths are measured in units of  $\xi_b$ .] Further, the dimensionless surface field in  $F_{S_1}$  is  $h_1 = -V(0)$ . The one-sided derivative appears in  $F_{S_1}$  due to the absence of neighboring atoms for  $z < 0$ . Similarly, the third term  $F_{S_2}$  is the contribution from the surface  $S_2$  located at  $z = D$ , with  $h_2 = -V(D)$ . For simplicity, we assume that  $J_{s_1} = J_{s_2} = J_s$ , so that the parameter  $g$  is the same for both  $S_1$  and  $S_2$ .

The corresponding dynamical model is obtained as follows. In the bulk, the order parameter evolves according to the Cahn-Hilliard-Cook (CHC) equation for a conserved order parameter [1, 2, 3, 4, 5, 41]:

$$\begin{aligned} \frac{\partial}{\partial t} \psi(\vec{r}, t) &= -\vec{\nabla} \cdot \vec{J}(\vec{r}, t) \\ &= \vec{\nabla} \cdot [\nabla \mu(\vec{r}, t) + \vec{\theta}(\vec{r}, t)] \\ &= \vec{\nabla} \cdot \left[ \vec{\nabla} \left( \frac{\delta F}{\delta \psi} \right) + \vec{\theta}(\vec{r}, t) \right]. \end{aligned} \quad (6)$$

Here,  $\vec{J}(\vec{r}, t)$  is the current, and  $\mu(\vec{r}, t)$  is the local chemical potential difference between A and B. Further,  $\vec{\theta}(\vec{r}, t)$  is a random noise term, to be specified below. Using the free energy functional from Eq. (3) in Eq. (6), we obtain

$$\frac{\partial}{\partial t} \psi(\vec{r}, t) = \vec{\nabla} \cdot \left\{ \vec{\nabla} \left[ -\psi + \psi^3 - \frac{1}{2} \nabla^2 \psi + V(z) \right] + \vec{\theta}(\vec{r}, t) \right\}, \quad 0 < z < D. \quad (7)$$

We assume that the noise  $\vec{\theta}$  is a Gaussian white noise, obeying the relations

$$\langle \vec{\theta}(\vec{r}, t) \rangle = 0, \quad (8)$$

$$\langle \theta_i(\vec{r}', t') \theta_j(\vec{r}'', t'') \rangle = 2\epsilon \delta_{ij} \delta(\vec{r}' - \vec{r}'') \delta(t' - t''). \quad (9)$$

The dimensionless noise amplitude is a function of the temperature [13]

$$\epsilon = \frac{1}{3} \left( \frac{T_c}{T} - 1 \right)^{-2} \xi_b^{-d} . \quad (10)$$

Eqs. (6)-(7) model the fact that the order parameter (the total concentration) is conserved [41]. However, it is important to note that the surface value of the order parameter is not a conserved quantity. We assume a nonconserved relaxational kinetics (referred to as *Model A* [41]) for this quantity at  $S_1$ :

$$\begin{aligned} \tau_0 \frac{\partial}{\partial t} \psi(\vec{\rho}, 0, t) &= - \frac{\delta F}{\delta \psi(\vec{\rho}, 0, t)} \\ &= h_1 + g\psi(\vec{\rho}, 0, t) + \gamma \frac{\partial \psi}{\partial z} \Big|_{z=0} , \end{aligned} \quad (11)$$

where  $\tau_0$  sets the time scale of the nonconserved kinetics. Since the surface value of the order parameter relaxes much faster than the time scales of phase separation, we subsequently set  $\tau_0 = 0$ . Finally, we observe that there is no current of material across  $S_1$ . This is implemented via a no-flux boundary condition:

$$J_z(\vec{\rho}, 0, t) = - \left\{ \frac{\partial}{\partial z} \left[ -\psi + \psi^3 - \frac{1}{2} \nabla^2 \psi + V(z) \right] + \theta_z \right\}_{z=0} = 0 . \quad (12)$$

The boundary conditions at  $z = D$  are implemented in a similar manner. For the sake of completeness, we present them here:

$$0 = h_2 + g\psi(\vec{\rho}, D, t) - \gamma \frac{\partial \psi}{\partial z} \Big|_{z=D} , \quad (13)$$

$$0 = \left\{ \frac{\partial}{\partial z} \left[ -\psi + \psi^3 - \frac{1}{2} \nabla^2 \psi + V(z) \right] + \theta(z) \right\}_{z=D} . \quad (14)$$

Eqs. (7)-(14) constitute our model for phase separation in a film [39]. This model has been presented in the context of a film with flat parallel surfaces. However, the adaptation to an arbitrary geometry is obvious: boundary conditions like Eqs. (11)-(14) are implemented on all available surfaces. For example, Aichmayer et al. [42] have used the appropriate generalization of this model to study SDSD in a cylindrical geometry.

We have undertaken a Langevin simulation of the above model, including the noise term, in order to study phase separation in both symmetric and antisymmetric films. We implemented an Euler-discretized version of Eqs. (7)-(14) on cubic

lattices of size  $L^2 \times D$  with  $L = 256$  and  $D = 5, 10$ . The discretization mesh sizes were  $\Delta x = 1$  and  $\Delta t = 0.02$ . We should stress that these mesh sizes are rather coarse and the resultant numerical solution does not closely shadow the “actual” solution of Eqs. (7)-(14). However, Oono and Puri [43] and Rogers et al. [44] have demonstrated that such discrete *cell-dynamical system* models capture the physics of the segregation process rather well. The boundary conditions in Eqs. (11)-(14) were implemented at  $z = 0$  and  $z = D$ , respectively, while periodic boundary conditions were applied in the  $x$ - and  $y$ -directions.

The nature of the surface potential  $V(z)$  and the parameters  $g, \gamma, \epsilon$  determine the equilibrium phase diagram of the film. For the semi-infinite case, the phase diagram has been discussed in Refs. [10, 13, 45]. For the films considered here, we have determined the boundary between PW and CW phases both analytically and numerically. For the sake of brevity, we do not discuss these phase diagrams here, but point out that parameter values are chosen to study ordering to both PW and CW states in symmetric and antisymmetric films. The values of the parameters in the boundary conditions were chosen as  $g = -0.4$ ,  $\gamma = 0.4$  [13]. The potentials  $V(z)$  which we considered will be specified at appropriate places in the subsequent discussion. The noise amplitude was fixed as  $\epsilon = 0.327$ , which corresponds to a quench with  $T \simeq 0.38 T_c$  from Eq. (10). The presence of thermal fluctuations prevents the system from becoming stuck in metastable configurations. However, we should stress that the ordering dynamics is expected to be independent of noise in the asymptotic regime [46, 47].

The initial conditions for our simulations consisted of a homogeneous mixture of 50% A and 50% B, i.e.,  $\psi(\vec{r}, t = 0) = 0 + \text{small-amplitude fluctuations}$ . This mimics the disordered high-temperature state for a mixture with critical composition. We will characterize the far-from-equilibrium dynamics of the quenched system via evolution snapshots, laterally averaged order parameter profiles, layer-wise correlation functions and length scales. All statistical quantities were obtained as averages over five independent runs.



### III. KINETICS OF PHASE SEPARATION IN A SYMMETRIC FILM

Let us first consider the case of a symmetric film with a power-law potential:

$$V(z) = -V_0 [(z+1)^{-3} + (D+1-z)^{-3}] \quad . \quad (15)$$

Recall that the exponent  $n = 3$  corresponds to non-retarded van der Waals' interactions between a surface and a particle in  $d = 3$ . As the other parameters are fixed, an appropriate choice of  $V_0$  and  $D$  results in either PW or CW states in equilibrium. We have ascertained the PW-CW phase boundary by studying the evolution of an initial condition which consists of A-rich and B-rich domains separated by an A-B interface along the  $z$ -direction. The onset of the CW phase is signaled by the intrusion of a thin wetting layer [see Fig. 1(b)] between the B-rich domain and the surfaces. We will consider the PW and CW cases separately.

#### A. Partially Wet Surfaces

In Fig. 2, we show evolution snapshots [part (a)] and  $(xz)$ -cross-sections [part (b)] for films with  $D = 5$  (frames on left) and  $D = 10$  (frames on right). The potentials were chosen with  $V_0 = 0.325$  for  $D = 5$  and  $V_0 = 0.11$  for  $D = 10$ , which correspond to the PW state in equilibrium. (The critical value of  $V_0/\sigma$  for the PW→CW crossover diminishes with increase in  $D$ , and  $V_0/\sigma \rightarrow 1$  as  $D \rightarrow \infty$ .) Note that a metastable layered structure forms at early times, since the kinetics of surface enrichment [48] is much faster than the time scale of phase separation. On longer time scales, spinodal fluctuations break this layered structure and the system forms domains which coarsen in directions parallel to the surface. We stress that the layered state can be very long-lived, and may be misinterpreted as evidence for the formation of wetting layers in experiments.

Many experimental probes (such as depth-profiling techniques) do not have any lateral resolution, and yield only laterally averaged order parameter profiles  $\psi_{\text{av}}(z, t)$  vs.  $z$  [9, 12]. In our simulations, laterally averaged profiles are obtained by averaging

$\psi(x, y, z, t)$  along the  $x$ - and  $y$ -directions, and then further averaging over five independent runs. The depth profiles corresponding to the evolution in Fig. 2 are shown in Fig. 3. For bulk spinodal decomposition, the wave-vectors are randomly oriented and the averaging procedure yields  $\psi_{\text{av}}(z, t) \simeq 0$ . For SDSD, however, the laterally averaged profiles are systematic at the surfaces since the boundary conditions result in spinodal waves with wave-vectors perpendicular to the surfaces. Let us focus on the case with  $D = 10$  in Fig. 3(b). The profile at time  $t = 10$  shows the formation of two symmetric SDSD waves, which propagate towards the center of the film. The  $t = 100$  profile shows the metastable layered state that has originated from these waves. This structure is also present at  $t = 1000$ , and may be misinterpreted as a CW equilibrium state which occurs for temperatures between the critical temperature of the thin film and the critical temperature of the bulk system [31, 32]. Finally, the spinodal fluctuations break this structure and the averaged profile at  $t = 20000$  is almost flat. Since a weak surface field amplitude  $V_0 = 0.11$  was chosen in this case, there is only a slightly A-rich region [ $\psi_{\text{av}}(z, t) > 0$ ] near the walls and, correspondingly, only a slightly A-poor region [ $\psi_{\text{av}}(z, t) < 0$ ] at the center.

It is also interesting to study  $(xy)$ -cross-sections of the evolution snapshots in Fig. 2. In Fig. 4, we show the relevant cross-sections at  $z = 2$  for  $D = 5$  and  $z = 5$  for  $D = 10$ . For early times ( $t = 100$ ) the central region is strongly depleted in A due to the formation of the layered structure. The resultant morphology corresponds to an off-critical composition with droplets of A in a matrix of B. At later times,  $t = 20000$ , the central region has almost equal amounts of A and B again. However, there is still a small depletion in A (see Fig. 3), and hence the growth morphology still contains droplets of A.

Let us next focus on the layer-wise correlation function, which is defined as [39]

$$C_{\parallel}(\vec{\rho}, z, t) = L^{-2} \int d\vec{\sigma} [\langle \psi(\vec{\sigma}, z, t) \psi(\vec{\sigma} + \vec{\rho}, z, t) \rangle - \langle \psi(\vec{\sigma}, z, t) \rangle \langle \psi(\vec{\sigma} + \vec{\rho}, z, t) \rangle] \quad , \quad (16)$$

where the angular brackets denote an averaging over independent runs. Since the system is isotropic in the  $(xy)$ -plane,  $C_{\parallel}$  does not depend on the direction of  $\vec{\rho}$ . We can define the  $z$ -dependent lateral length scale  $L_{\parallel}(z, t) \equiv L(z, t)$  from the half-decay

of  $C_{\parallel}(\rho, z, t)$  [39]:

$$C_{\parallel}(\rho = L, z, t) = \frac{1}{2}C_{\parallel}(0, z, t). \quad (17)$$

For convenience, we denote  $C_{\parallel}(\rho, z, t)$  as  $C(\rho, t)$  in the following discussion. In Figs. 5(a),(b) we plot the scaled correlation functions  $C(\rho, t)/C(0, t)$  vs.  $\rho/L$  for  $D = 5$  and  $D = 10$ , respectively. In bulk systems, the correlation function exhibits *dynamical scaling*, viz.,  $C(\vec{r}, t) = g(r/L)$ , where  $g(x)$  is independent of time. This property indicates that the evolution morphology is statistically self-similar in time, and only the scale of the morphology changes. In this case, there is no dynamical scaling as the correlation functions correspond to qualitatively different morphologies (see Fig. 2). Thus, for  $D = 10$  and  $t = 1000$ , the layered structure has not yet broken up, while at  $t = 20000$  lateral phase separation has occurred. Of course, dynamical scaling is recovered subsequent to the formation of well-formed laterally segregated domains ( $t \geq 10000$  for both  $D = 5$  and 10).

Finally, we examine the time-dependence of the lateral domain size  $L(z, t)$  in Fig. 6. While the asymptotic growth is consistent with the expected Lifshitz-Slyozov (LS) growth law  $L(t) \sim t^{1/3}$  [1, 2, 3, 4, 5], which describes bulk domain growth, the early-time dynamics is complicated. For the  $D = 10$  case in Fig. 6(b), the early-time data corresponds to the growth of bulk-like domains before the layered structure has formed. The spinodal fluctuations originate in the central region ( $z = 5$ ) where the surface field is not felt, and propagate to the surface ( $z = 0$ ). The break-up of the layered structure is characterized by the non-monotonic behavior of  $L(z, t)$  vs.  $t$ . As the fluctuations originate near the film center, the data set for  $z = 0$  is the last to become consistent with LS behavior.

## B. Completely Wet Surfaces

Next, let us consider the case where the surfaces have a CW morphology in equilibrium. In Fig. 7, we show evolution snapshots and  $(xz)$ -cross-sections for the CW case. The corresponding potential strengths were  $V_0 = 0.45$  for  $D = 5$ , and  $V_0 = 0.275$  for  $D = 10$ . Again, the system forms a metastable layered structure at early

times, which is broken up by spinodal fluctuations at later times. (For very strong surface fields, the layered structure actually corresponds to an equilibrium state and the corresponding pattern dynamics is uninteresting.) However, the difference in this case is that the B-rich regions are encapsulated by A [see Fig. 1(b)], unlike the situation shown in Fig. 2. The asymptotic dynamics is then characterized by the coarsening of these encapsulated pancakes. The laterally averaged profiles (Fig. 8) again show that the initial layered structure is rather pronounced (compare with Fig. 3). The depth profiles become softer at later times, but due to the pancakes being encapsulated by A, there remains a strong surface enrichment in A. If one looks at cross-sections taken parallel to the surfaces, analogous to Fig. 4, one finds a qualitatively similar behavior. Of course, the volume fraction of A in the central region is now smaller due to the higher degree of surface enrichment.

Figure 9 is a scaling plot of  $C(\rho, t)/C(0, t)$  vs.  $\rho/L$ , and is analogous to Fig. 5. We do not show data for the  $z = 0$  case here as the surface is always A-rich and does not exhibit interesting pattern dynamics. The behavior in the film center is qualitatively similar to the PW case, i.e., there is no dynamical scaling for the time range shown. This can be understood in the context of the evolution dynamics shown in Fig. 7(b). For the  $D = 10$  case, the morphologies exhibit a crossover behavior from the layered state to the (asymptotic) pancake state for  $t = 100, 1000, 20000$ . For  $t \geq 20000$ , we expect to recover dynamical scaling. For the  $D = 5$  case, the system is almost in its asymptotic state by  $t = 1000$ . Hence, the correlation functions for  $t = 1000$  and  $t = 20000$  show approximate scaling.

In Fig. 10, we study the time-dependence of the parallel length scale  $L(z, t)$ . The non-monotonic behavior again reflects the formation and break-up of a long-lived metastable layered structure. Notice that this state is far from equilibrium despite the fact that we do expect a CW morphology for these parameter values. The break-up of the layered structure gives rise to the growth of laterally segregated domains. Although we have followed the growth of  $L(z, t)$  over several decades in time, the expected asymptotic regime of LS growth is not observed over simulation time-scales.

## IV. KINETICS OF PHASE SEPARATION IN AN ANTISYMMETRIC FILM

We next consider the case of an antisymmetric film. The corresponding power-law potential is

$$V(z) = -V_0 [(z + 1)^{-3} - (D + 1 - z)^{-3}], \quad (18)$$

so that  $V(D - z) = -V(z)$ . In Figs. 1(c)-(d), we have schematically shown the PW and CW states which arise for an antisymmetric film. In this case also, we have obtained the PW-CW phase boundary as a function of  $V_0$  and  $D$ . As before, we will consider and compare both PW and CW cases.

### A. Partially Wet Surfaces

In Fig. 11, we show evolution snapshots [part (a)] and  $(xz)$ -cross-sections [part (b)] for films with  $D = 5$  (frames on left) and  $D = 10$  (frames on right). The potential strengths were  $V_0 = 0.055$  for  $D = 5$  and  $V_0 = 0.041$  for  $D = 10$ , which correspond to a PW case in equilibrium. In the  $D = 5$  case, we observe the formation of a layered state which breaks up into a coarsening domain structure. A similar evolution occurs in the  $D = 10$  case, though the layered state (at  $t = 1000$ ) is not so clean for these weak surface fields. However, it shows up more clearly in the laterally averaged profiles we present next. The domain cross-sections are trapezoidal with different contact angles at the lower surface (which prefers A) and the upper surface (which prefers B).

The laterally averaged profiles (Fig. 12) confirm that a layered state, with a single interface, appears as a transient before the lateral domain growth sets in. For the  $D = 10$  case, we see the interaction of two opposite SDSD waves (at  $t = 10, 100$ ), resulting in the formation of the layered state (at  $t = 1000$ ). In Fig. 13, we examine the morphology in planes parallel to the surfaces. For the  $D = 5$  case, we focus on a cross-section at  $z = 2$ . The  $t = 100$  morphology corresponds to the layered state [see Fig. 12(a)] and consists of droplets of B in a matrix of A. The  $t = 20000$  morphology

corresponds to the laterally-segregated state and consists of bicontinuous domains. For the  $D = 10$  case, we consider a cross-section at  $z = 5$ , which is precisely the film center. Since the film always has a near-critical composition at the center [see Fig. 12(b)], the segregation morphology is bicontinuous for both  $t = 100$  and  $t = 20000$  in this case.

We have also examined the layer-wise correlation functions  $C_{\parallel}(\vec{\rho}, z, t) \equiv C(\rho, t)$  (Fig. 14), and the lengths  $L(z, t)$  which one can extract from them (Fig. 15). Again, one finds marked deviations from scaling for  $C(\rho, t)$ , as expected due to the transient formation of layered structures. Of course, scaling is recovered in the asymptotic regime, which is characterized by the coarsening of trapezoidal domains. In the  $D = 5$  case, the length-scale data shows that the asymptotic behavior is consistent with the LS law,  $L(t) \sim t^{1/3}$ . A similar behavior is seen for the film with  $D = 10$ , though the non-monotonic behavior is less pronounced in this case. This emphasizes that one has to be careful with the interpretation of growth phenomena in confined geometries, and rather complete information on the structural evolution of a system is mandatory for establishing a clear picture.

## B. Completely Wet Surfaces

Our last set of numerical results corresponds to the CW state for an antisymmetric film: in this case, a layered state with a single interface is the equilibrium state [see Fig. 1(d)], and no lateral segregation should occur! In Fig. 16, we show evolution snapshots and  $(xz)$ -cross-sections for  $D = 5$  with  $V_0 = 0.25$  (frames on left) and  $D = 10$  with  $V_0 = 0.2$  (frames on right). There is seen to be some lateral inhomogeneity in the early stages. Starting from a random initial state, small A-rich and B-rich domains are formed first. It takes time for the interfaces between these small domains to annihilate by diffusion and coalescence, until a single domain wall parallel to the surface is left. The corresponding laterally averaged profiles are shown in Fig. 17. In particular, we draw the reader's attention to Fig. 17(b), which shows the formation and collision of two opposite SDS waves originating from  $S_1$

and  $S_2$  – see profiles for  $t = 10$  and  $t = 100$ . Figure 18 shows the evolution pictures at the film center ( $z = 5$ ) for the  $D = 10$  case. (The corresponding pictures at  $z = 2$  or  $z = 3$  for the  $D = 5$  case merely show a uniform state.) The length scale at  $z = 5$  for  $D = 10$  (Fig. 19) grows uniformly for  $t \geq 1000$ , and the time-dependence is consistent with the LS law.

## V. SUMMARY AND DISCUSSION

Let us conclude this paper with a summary and discussion of the results. We have studied the diffusion-driven phase separation of an AB mixture confined in a film. The film has two parallel surfaces  $S_1$  and  $S_2$ , which are separated by a distance  $D \sim O(10\xi_b)$ , where  $\xi_b$  is the bulk correlation length. We have considered (a) *symmetric films*, where  $S_1$  and  $S_2$  have an identical attraction for the A-component; and (b) *antisymmetric films*, where  $S_1$  and  $S_2$  attract (with equal strength) the A-component and B-component, respectively. Both cases are of considerable experimental relevance.

The equilibrium segregated state can be either partially wet (PW) or completely wet (CW), depending on the nature of the surface potentials. Further types of mixed-phase states in thin films occur only for restricted ranges of parameters [34, 35, 36], and are not considered in the present paper. We have clarified the typical growth scenario in both symmetric and antisymmetric films. In both PW and CW cases, the surfaces give rise to surface-directed spinodal decomposition (SDSD) waves, which propagate towards the film center. The interaction of these SDSD waves leads to the formation of a layered state. This state is metastable for the PW case, and is broken up by spinodal fluctuations. (However, the metastable state may have a very long lifetime, and could be of considerable experimental significance.) The subsequent evolution of the mixture is characterized by the lateral coarsening of pancake-like domains. (For antisymmetric films, these domains are trapezoidal because of the different contact angles at  $S_1$  and  $S_2$ .) In the later stages, we expect that this coarsening is governed by the Lifshitz-Slyozov (LS) growth law  $L(t) \sim t^{1/3}$ , but one

often encounters slow transients and even a non-monotonic variation of  $L(t)$  with time, before the LS regime sets in. For the CW case in symmetric films, the initial layered state is again metastable for moderate surface fields, and breaks up into encapsulated pancakes which coarsen in the lateral direction. For the CW case in antisymmetric films, the equilibrium state is a layered state with a single interface parallel to the surfaces. The system can relax to this state rather rapidly.

At this stage, one may ask what happens if hydrodynamic effects are incorporated into the above discussion. It is well-known [1, 2, 3, 4, 5] that bulk fluid mixtures exhibit more complicated segregation kinetics than solid mixtures. In the initial stages, growth is diffusive and is governed by the LS growth law. However, at later times, hydrodynamic effects become relevant and domain growth is facilitated by advective transport along interfaces. The corresponding growth laws are  $L(t) \sim t$  in the *viscous hydrodynamic* regime [49], and  $L(t) \sim t^{2/3}$  in the *inertial hydrodynamic* regime [50]. The effects of surfaces on phase-separating binary fluids can be studied at various levels of description. At the coarse-grained level, an appropriate model is *Model H* at a surface [41, 51]. This consists of the coupled dynamics of an order-parameter field and a velocity field, with appropriate boundary conditions at the surfaces. Alternatively, one can study mesoscale models consisting, e.g., of evolution equations for the configuration probability distribution [52]. Finally, at the microscopic level, one can undertake molecular dynamics (MD) simulations of binary fluids [53] in a confined geometry. We have undertaken such MD simulations, and will report the results in a forthcoming publication.

More generally, we emphasize that there are many intriguing aspects of phase separation in confined geometries, and a number of possible directions for further investigation. For example, the present study focused on mixtures with critical composition. In a semi-infinite geometry, Puri and Binder [54] have demonstrated that novel features arise when off-critical compositions are considered, e.g., the wetting layer grows faster when the wetting component is a minority phase rather than a majority phase. It would also be interesting to study the phase separation of off-critical mixtures in the present context of confined geometries. Another inter-



esting complication arises if there is frozen-in disorder at the surfaces, which affects the wetting behavior. Finally, it is also relevant to study SDSA in more complex confined geometries than those studied here, e.g., wedges, patterned surfaces, etc. Though the modeling of these problems is straightforward, we expect that they will give rise to novel physical phenomena. There remain many issues to be addressed in this area, and we urge experimentalists to undertake fresh experiments in these directions.

**Acknowledgments:** SKD received financial support from the Deutsche Forschungsgemeinschaft (DFG) via grant No Bi314/18-2. JH acknowledges support from the Emmy Noether Program at the DFG. SP is grateful to K. Binder for inviting him to Mainz, where this work was initiated. Furthermore support from the DFG via Sonderforschungsbereich 625/A3 is acknowledged.

- 
- [1] J. D. Gunton, M. San Miguel, and P. S. Sahni, In *Phase Transition and Critical Phenomena, Vol 8*, C. Domb and J. L. Lebowitz, eds. (Academic Press, London, 1983) p. 267.
  - [2] S. Komura and H. Furukawa, eds., *Dynamics of Ordering Processes in Condensed Matter* (Plenum Press, New York, 1988).
  - [3] K. Binder and P. Fratzl, in *Phase Transformations in Materials*, G. Kostorz, ed., (Wiley-VCH, Weinheim, 2001) p. 409.
  - [4] A. Onuki, *Phase Transition Dynamics* (Cambridge Univ. Press, Cambridge, 2002).
  - [5] S. Dattagupta and S. Puri, *Dissipative Phenomena in Condensed Matter: Some Applications* (Springer, Berlin, in press).
  - [6] R. A. L. Jones, L. J. Norton, E. J. Kramer, F. S. Bates, and P. Wiltzius, *Phys. Rev. Lett.* **66**, 1326 (1991).
  - [7] S. Puri and K. Binder, *Phys. Rev. A* **46**, R4487 (1992); *Phys. Rev. E* **49**, 5359 (1994).
  - [8] G. Brown and A. Chakrabarti, *Phys. Rev. A* **46**, 4829 (1992).

- [9] G. Krausch, Mater. Sci. Eng. Rep. R **14**, 1 (1995).
- [10] S. Puri and H. L. Frisch, J. Phys.: Condens. Matter **9**, 2109 (1997).
- [11] K. Binder, J. Non-Equilib. Thermodyn. **23**, 1 (1998).
- [12] M. Geoghegan and G. Krausch, Progr. Polym. Sci. **28**, 261 (2003).
- [13] S. Puri, J. Phys.: Condens. Matter **17**, R1 (2005).
- [14] K. Binder, In *Phase Transitions and Critical Phenomena, Vol. 8*, C. Domb and J. L. Lebowitz (Academic Press, London, 1983), p. 1.
- [15] H. W. Diehl, In *Phase Transitions and Critical Phenomena, Vol. 10*, C. Domb and J. L. Lebowitz, eds. (Academic Press, London, 1986) p. 75.
- [16] J. W. Cahn, J. Chem. Phys. **66**, 3667 (1977).
- [17] M. E. Fisher, J. Stat. Phys. **34**, 667 (1984); J. Chem. Soc. Faraday Trans. **282**, 1569 (1986).
- [18] P. G. de Gennes, Rev. Mod. Phys. **57**, 827 (1985).
- [19] D. E. Sullivan and M. M. Telo da Gama, in *Fluid Interfacial Phenomena*, C. A. Croxton, ed. (Wiley, New York, 1986), p. 45.
- [20] S. Dietrich, in *Phase Transitions and Critical Phenomena, Vol. 12*, C. Domb and J. L. Lebowitz, eds. (Academic Press, London, 1988) p. 1.
- [21] M. Schick, in *Liquids at Interfaces*, J. Charvolin, J. F. Joanny, and J. Zinn-Justin, eds. (North-Holland, Amsterdam, 1990) p. 415.
- [22] K. Binder, D. P. Landau and M. Müller, J. Stat. Phys. **110**, 1411 (2003).
- [23] D.M. Kroll and G. Gompper, Phys. Rev. B **39**, 433 (1989).
- [24] K. Binder, Ann. Rev. Phys. Chem. **43**, 33 (1992).
- [25] K. Binder and D. P. Landau, J. Chem. Phys. **96**, 1444 (1992).
- [26] M.E. Fisher and H. Nakanishi, J. Chem. Phys. **75**, 5857 (1981); H. Nakanishi and M. E. Fisher, J. Chem. Phys. **78**, 3279 (1983).
- [27] R. Evans, J. Phys.: Condens. Matter **2**, 8989 (1990).
- [28] L. D. Gelb, K. E. Gubbins, R. Radhakrishnan, and M. Sliwinski-Bartkowiak, Rep. Prog. Phys. **62**, 1573 (1999).
- [29] M. Müller and K. Binder, J. Phys.: Condens. Matter **17**, S333 (2005).

- [30] Y. Rouault, J. Baschnagel, and K. Binder, *J. Stat. Phys.* **80**, 1009 (1995).
- [31] T. Flebbe, B. Dünweg, and K. Binder, *J. Phys. II France* **6**, 667 (1996).
- [32] K. Binder, P. Nielaba, and V. Pereyra, *Z. Phys. B* **104**, 81 (1997).
- [33] M. Müller and K. Binder, *Macromolecules* **31**, 8323 (1998).
- [34] M. Müller, K. Binder, and E. V. Albano, *Physica A* **279**, 188 (2000); *Int. J. Mod. Phys. B* **15**, 1867 (2001).
- [35] M. Müller, K. Binder, and E. V. Albano, *Europhys. Lett.* **50**, 724 (2000); M. Müller and K. Binder, *Phys. Rev. E* **63**, 021602 (2001).
- [36] K. Binder, M. Müller, and E. V. Albano, *Phys. Chem. Chem. Phys.* **3**, 1160 (2001).
- [37] T. Young, *Philos. Trans. R. Soc. London, Ser. A* **95**, 69 (1805).
- [38] A.J. Liu, D.J. Dorian, E. Herbolzheimer, and S.A. Safran, *Phys. Rev. Lett.* **65**, 1897 (1990); L. Monette, A.J. Liu, and G.S. Grest, *Phys. Rev. A* **46**, 7664 (1992).
- [39] S. Puri and K. Binder, *J. Stat. Phys.* **77**, 145 (1994).
- [40] I.E. Dzyaloshinskii, E.M. Lifshitz and L.P. Pitaevskii, *Adv. Phys.* **10**, 165 (1961).
- [41] P.C. Hohenberg and B.I. Halperin, *Rev. Mod. Phys.* **49**, 435 (1977).
- [42] B. Aichmayer, P. Fratzl, S. Puri and G. Saller, *Phys. Rev. Lett.* **91**, 015701 (2003).
- [43] Y. Oono and S. Puri, *Phys. Rev. Lett.* **58**, 836 (1987); *Phys. Rev. A* **38**, 434 (1988); S. Puri and Y. Oono, *Phys. Rev. A* **38**, 1542 (1988).
- [44] T.M. Rogers, K.R. Elder and R.C. Desai, *Phys. Rev. B* **37**, 9638 (1988).
- [45] S. Puri and K. Binder, *Z. Phys. B* **86**, 263 (1992).
- [46] S. Puri and Y. Oono, *J. Phys. A* **21**, L755 (1988).
- [47] A.J. Bray, *Phys. Rev. Lett.* **62**, 2841 (1989).
- [48] S. Puri and H.L. Frisch, *J. Chem. Phys.* **99**, 5560 (1993); H.L. Frisch, S. Puri, and P. Nielaba, *J. Chem. Phys.* **110**, 10514 (1999); K. Binder and H.L. Frisch, *Z. Phys. B* **84**, 403 (1991).
- [49] E.D. Siggia, *Phys. Rev. A* **20**, 595 (1979).
- [50] H. Furukawa, *Phys. Rev. A* **31**, 1103 (1985).
- [51] H. Tanaka, *J. Phys.: Condens. Matter* **13**, 4637 (2001).
- [52] S. Bastea, S. Puri, and J.L. Lebowitz, *Phys. Rev. E* **63**, 041513 (2001).

- [53] S.K. Das, J. Horbach, and K. Binder, J. Chem. Phys. **119**, 1547 (2003).
- [54] S. Puri and K. Binder, Phys. Rev. Lett. **86**, 1797 (2001); Phys. Rev. E **66**, 061602 (2002).

## Figures and Figure Captions

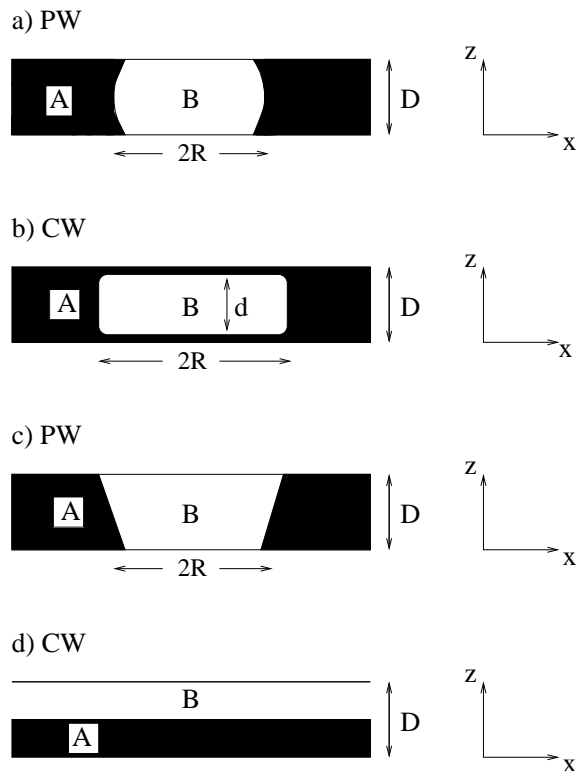


FIG. 1: Schematic description of phase-separated states in thin films of volume  $L \times L \times D$ . We show cross-sections of the film in the  $(xz)$ -plane. Cases (a)-(b) refer to thin films where both surfaces prefer A, and the surface potential is symmetric,  $V(D - z) = V(z)$ . Cases (c)-(d) refer to thin films where the lower surface prefers the A-rich phase and the upper surface prefers the B-rich phase. The corresponding surface potential is antisymmetric,  $V(D - z) = -V(z)$ . The A-rich domains are marked black, and the B-rich domains are unmarked. For both symmetric and antisymmetric films, partially wet (PW) and completely wet (CW) morphologies emerge in the limit  $D \rightarrow \infty$ . Further types of phase-separated states exist in thin films at off-critical composition [34, 35, 36], but we will not consider these here. Note that the thickness  $d$  of the encapsulated B-rich domain in (b) differs from  $D$  only by corrections which increase slower than linearly with  $D$ .

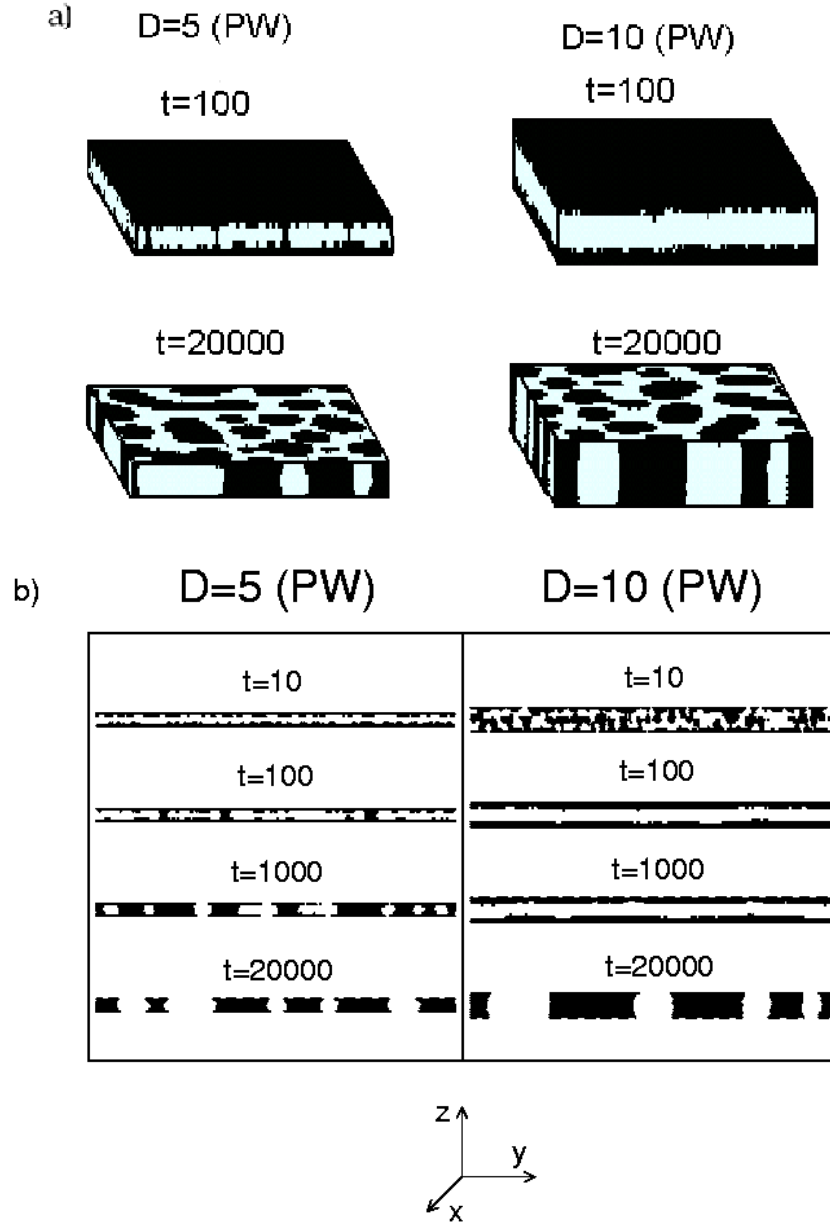


FIG. 2: (a) Evolution snapshots at times  $t = 100$  and  $t = 20000$  for a critical binary mixture in a symmetric film with PW morphology. The system size was  $L^2 \times D$  with  $L = 256$  and  $D = 5$  (frames on left) and  $D = 10$  (frames on right). The A-rich regions are colored black, and the B-rich regions are colored white (light blue online). (b) Perpendicular cross-sections of the snapshots in (a) at  $y = L/2$  in the  $(xz)$ -plane. The A-rich regions are marked black, and the B-rich regions are unmarked.

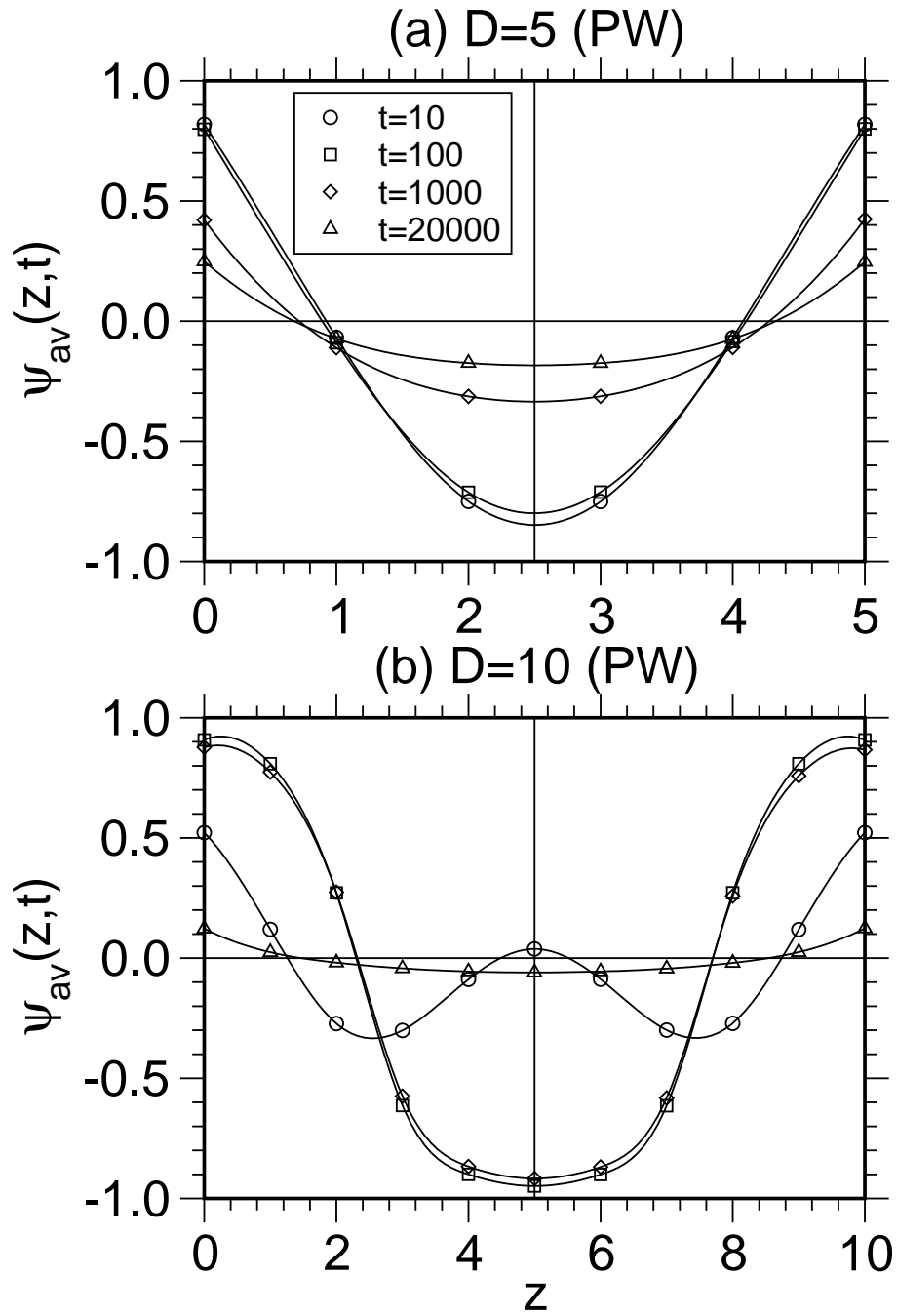


FIG. 3: Laterally averaged profiles for the evolution depicted in Fig. 2 at the dimensionless times  $t = 10, 100, 1000, 20000$ , for (a)  $D = 5$ , and (b)  $D = 10$ . The symbols denote the same times in both figures.

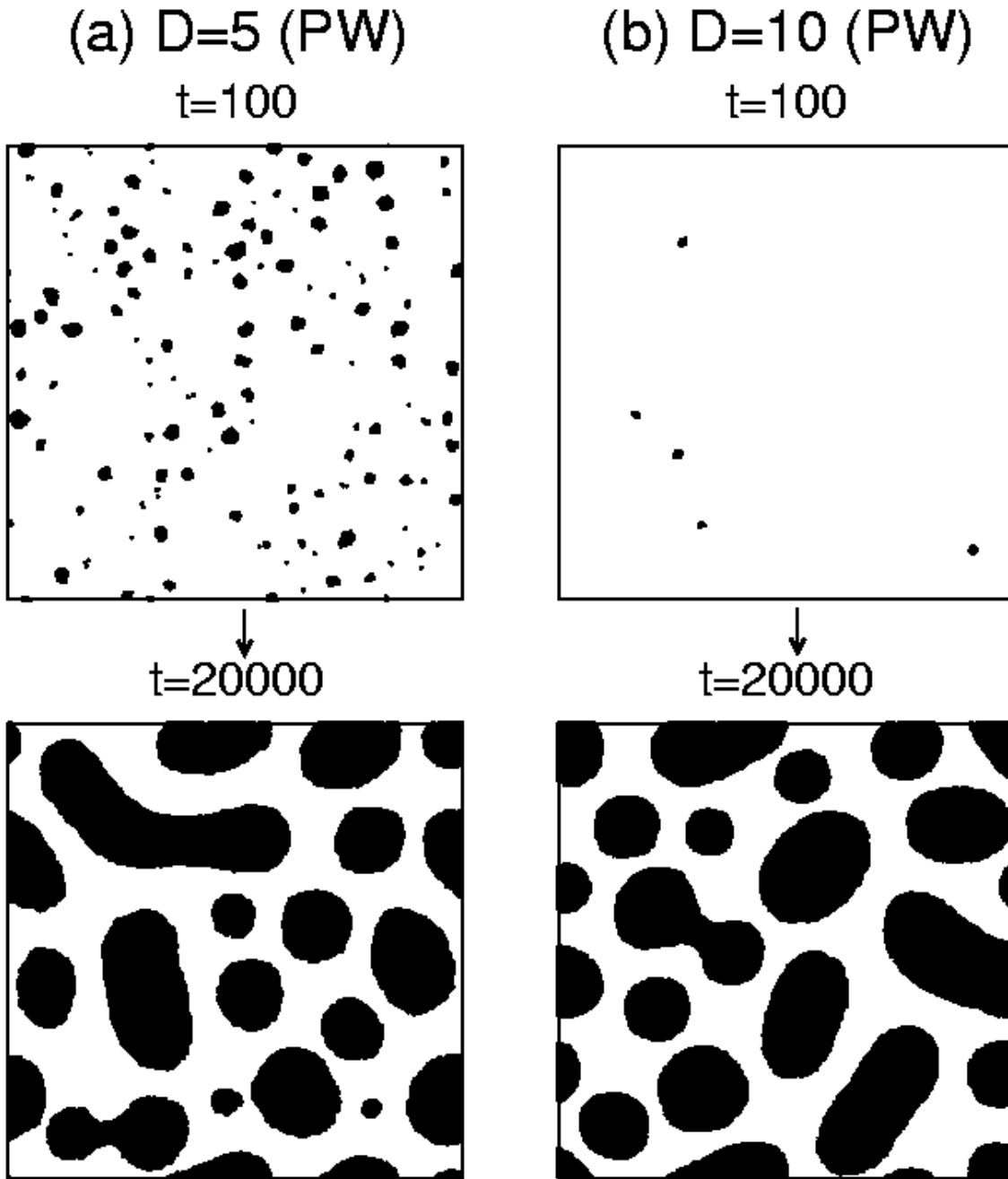


FIG. 4: Cross-sections of the evolution snapshots in Fig. 2(a). The cross-sections are taken parallel to the surfaces at (a)  $z = 2$  for  $D = 5$ , and (b)  $z = 5$  for  $D = 10$ .



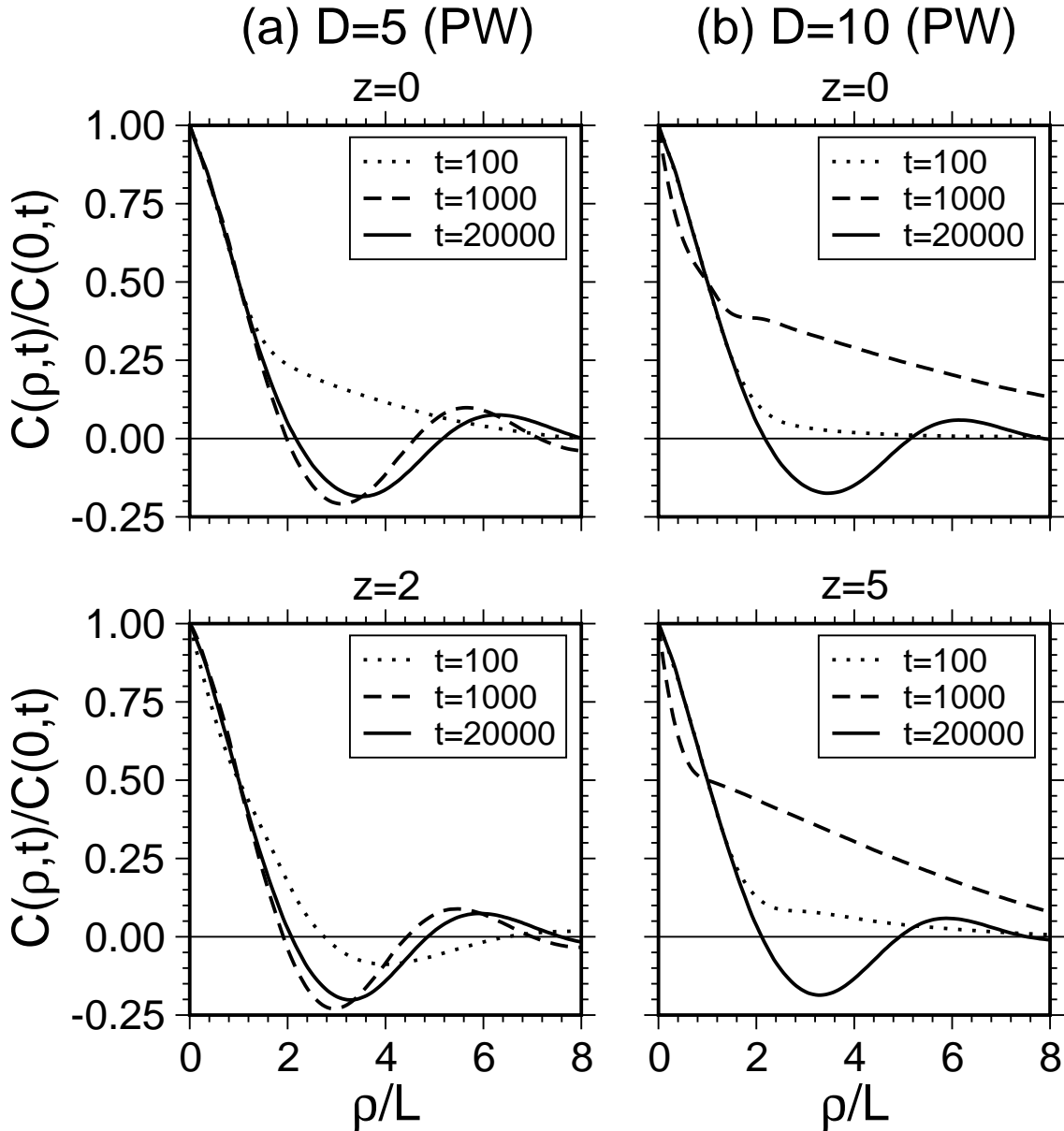


FIG. 5: Scaling plot of layer-wise correlation functions, defined in Eq. (16), for the evolution depicted in Fig. 2. We plot data for  $C(\rho, t)/C(0, t)$  vs.  $\rho/L$  for three different times,  $t = 100, 1000, 20000$ . We present data for (a)  $D = 5$  at  $z = 0$  (wall) and  $z = 2$  (center); and (b)  $D = 10$  at  $z = 0$  (wall) and  $z = 5$  (center). The layer-wise length-scale  $L(z, t)$  is defined as the distance over which  $C(\rho, t)$  has decayed to  $1/2$  its maximum value (at  $\rho = 0$ ).

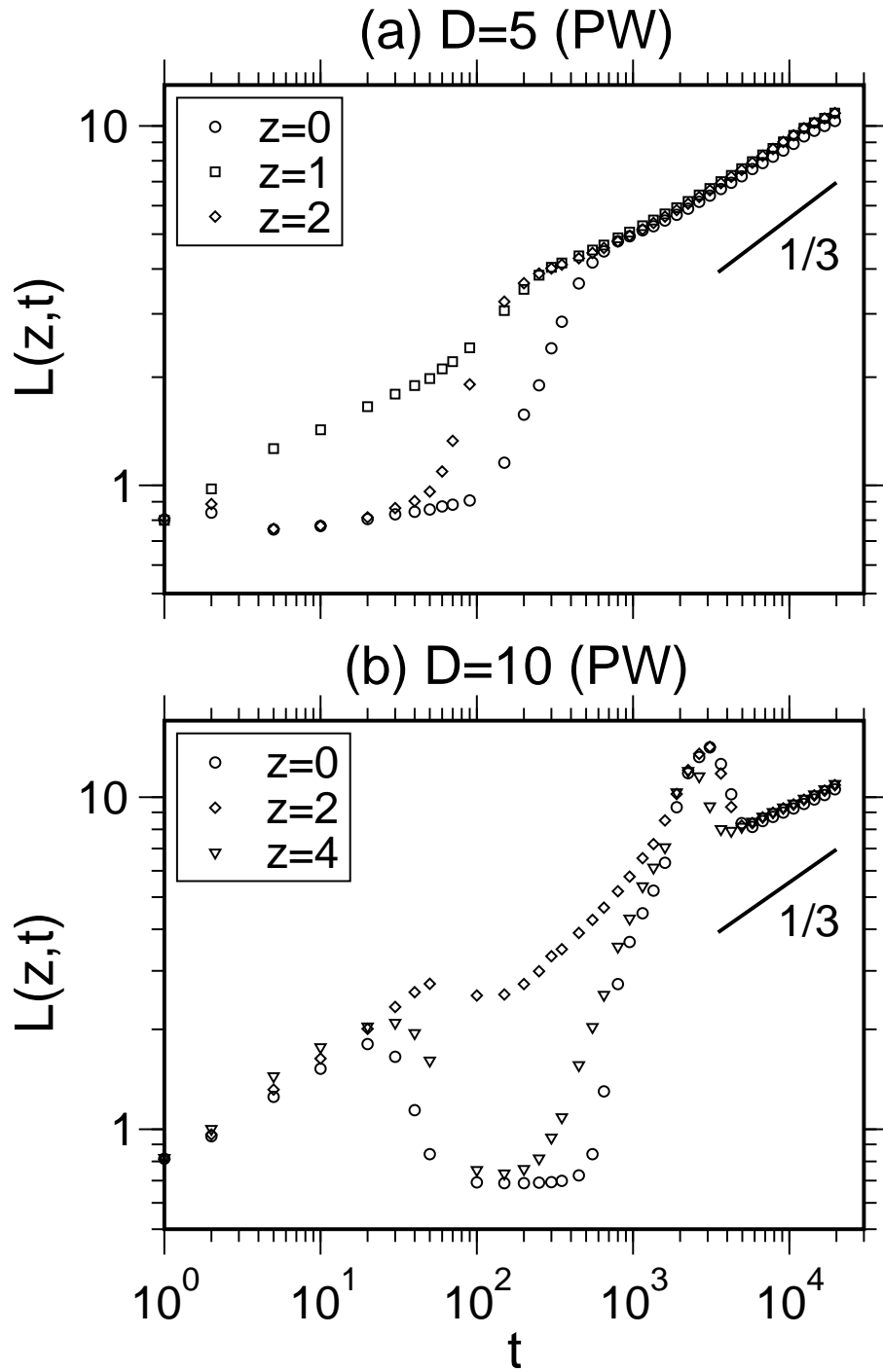


FIG. 6: Time-dependence of the layer-wise length scale for the evolution depicted in Fig. 2. We plot  $L(z,t)$  vs.  $t$  on a log-log scale for various values of  $z$  and (a)  $D = 5$ , and (b)  $D = 10$ . The lines of slope  $1/3$  denote the Lifshitz-Slyozov (LS) growth law,  $L(t) \propto t^{1/3}$ , which characterizes diffusion-driven phase separation in the bulk.

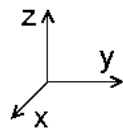
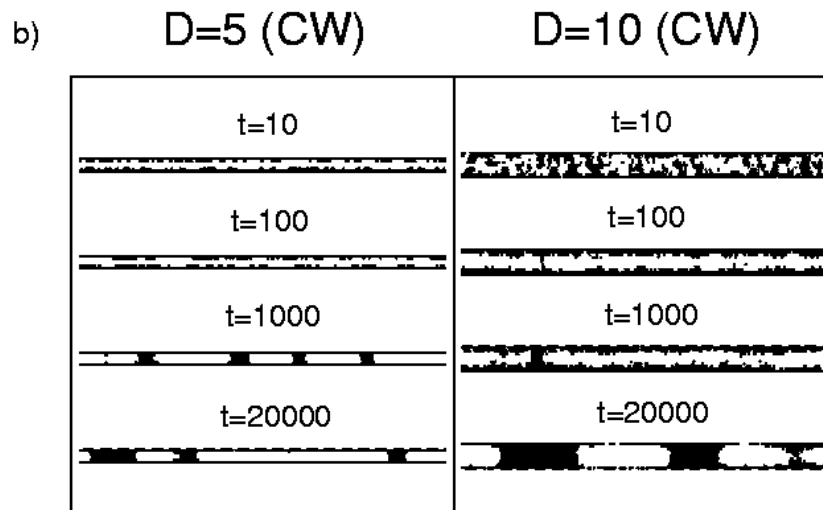
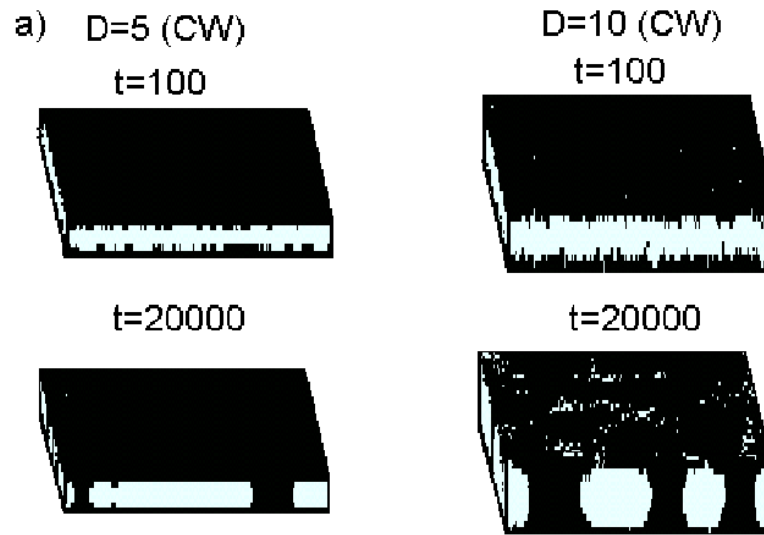


FIG. 7: Analogous to Fig. 2, but for a symmetric film with a CW morphology. The parameter values are just above the PW-CW boundary for the  $D = 10$  case. Therefore, the surface does not have a clean coating of the A-rich phase.

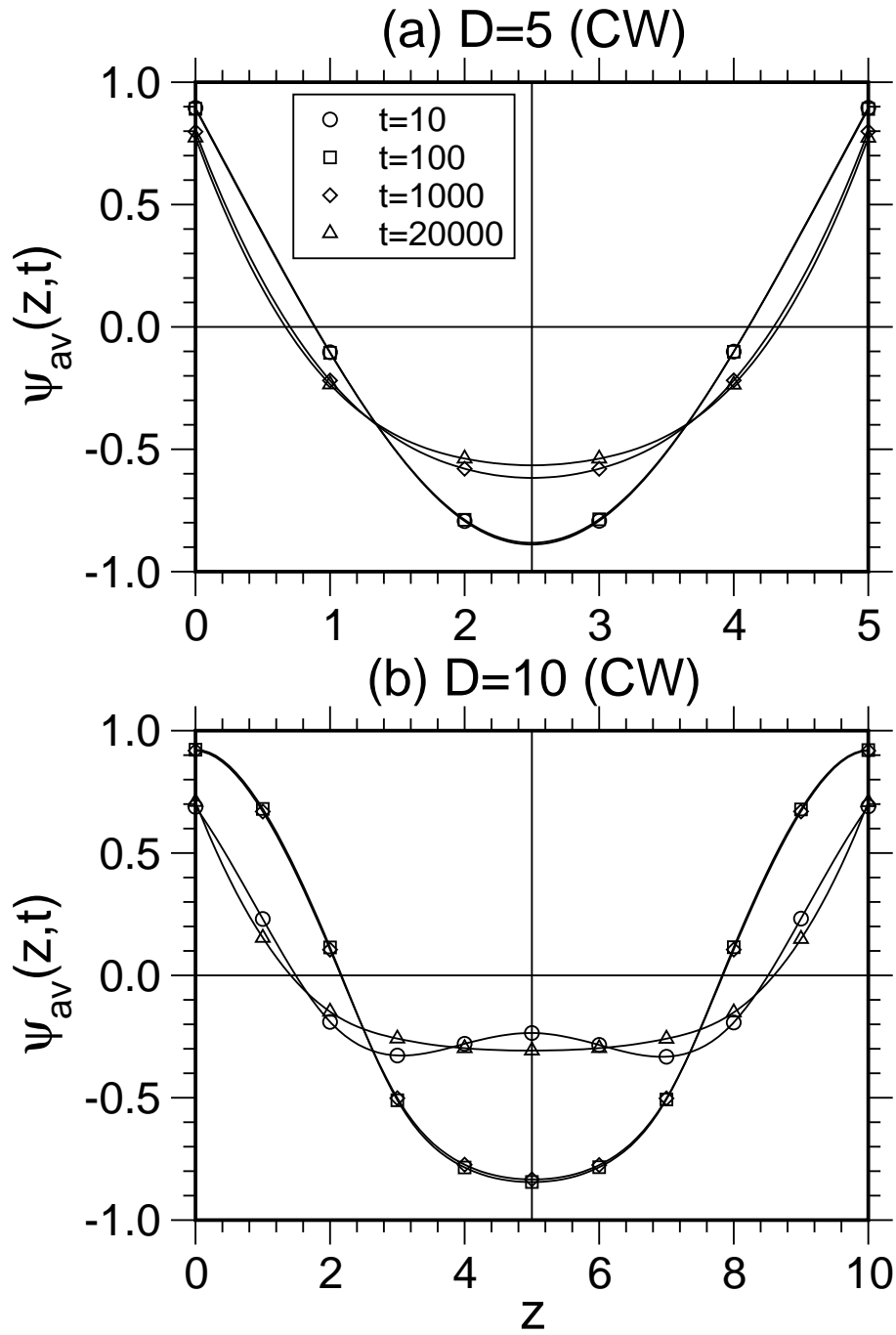


FIG. 8: Laterally averaged profiles for the evolution depicted in Fig. 7 at the dimensionless times  $t = 10, 100, 1000, 20000$ , for (a)  $D = 5$ , and (b)  $D = 10$ .

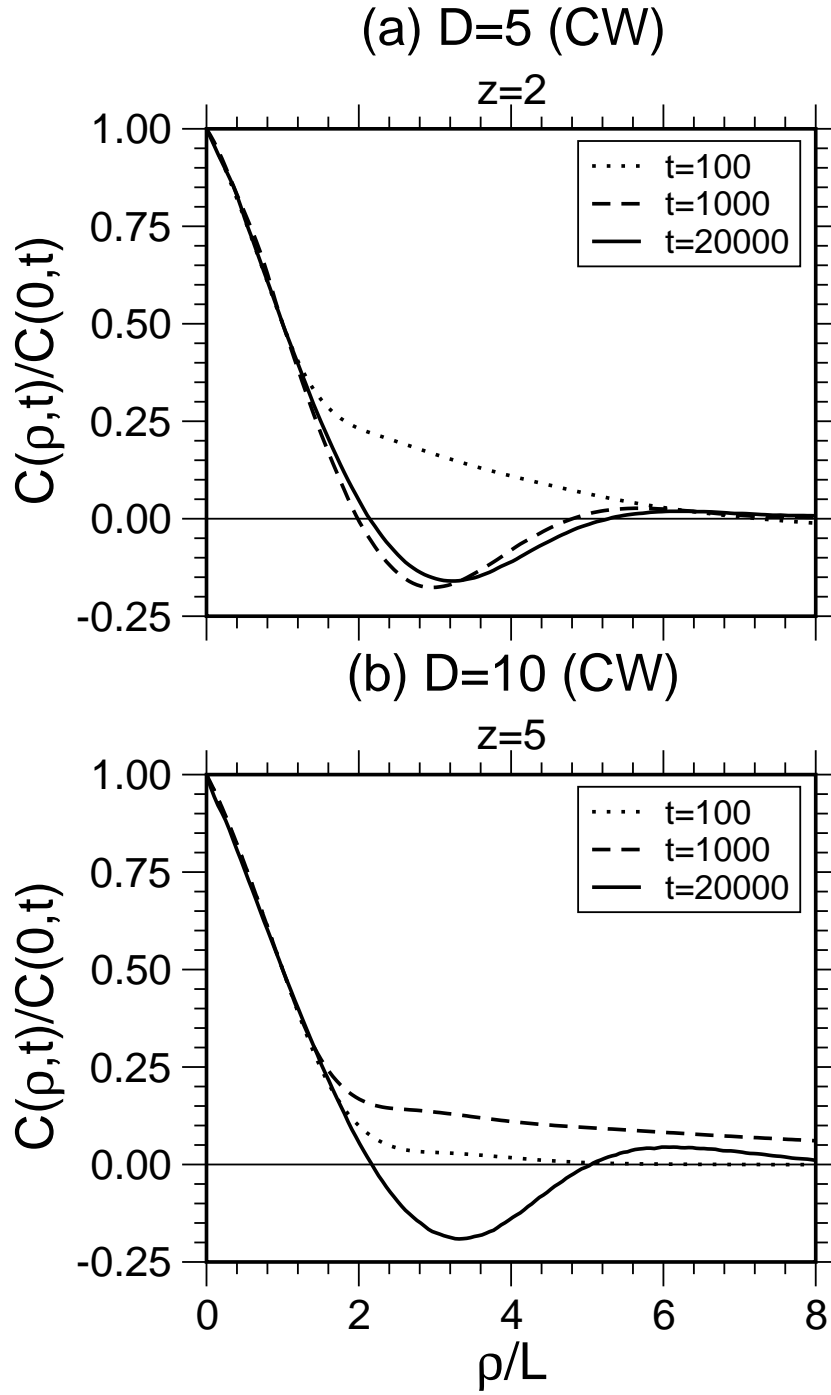


FIG. 9: Scaling plot of layer-wise correlation functions for the evolution depicted in Fig. 7. We plot  $C(\rho, t)/C(0, t)$  vs.  $\rho/L$  for  $t = 100, 1000, 20000$ . We present data for (a)  $D = 5$  at  $z = 2$  (center); and (b)  $D = 10$  at  $z = 5$  (center).

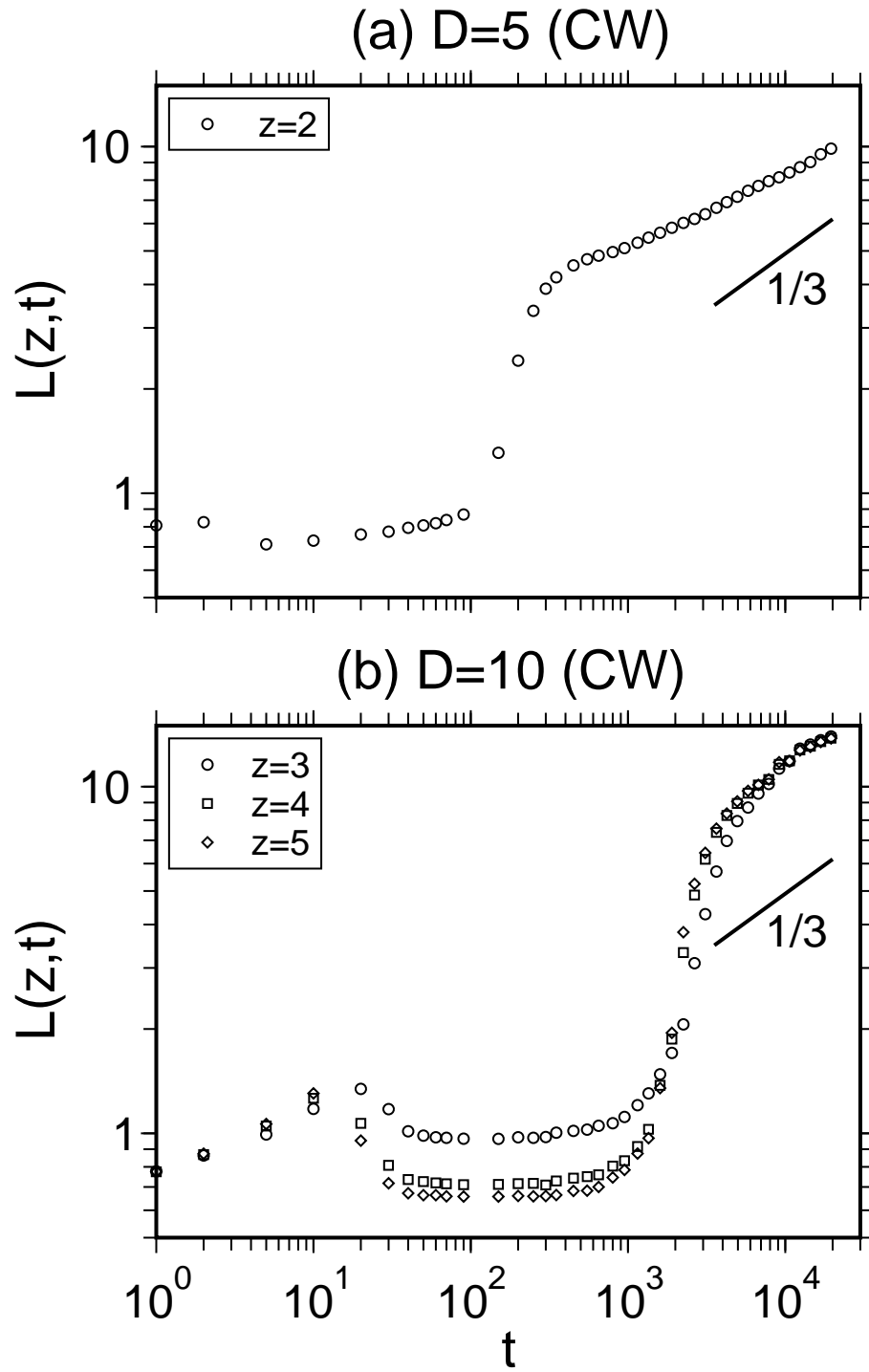


FIG. 10: Time-dependence of the layer-wise length scale for the evolution depicted in Fig. 7. We plot  $L(z, t)$  vs.  $t$  on a log-log scale for various values of  $z$  and (a)  $D = 5$ , and (b)  $D = 10$ .

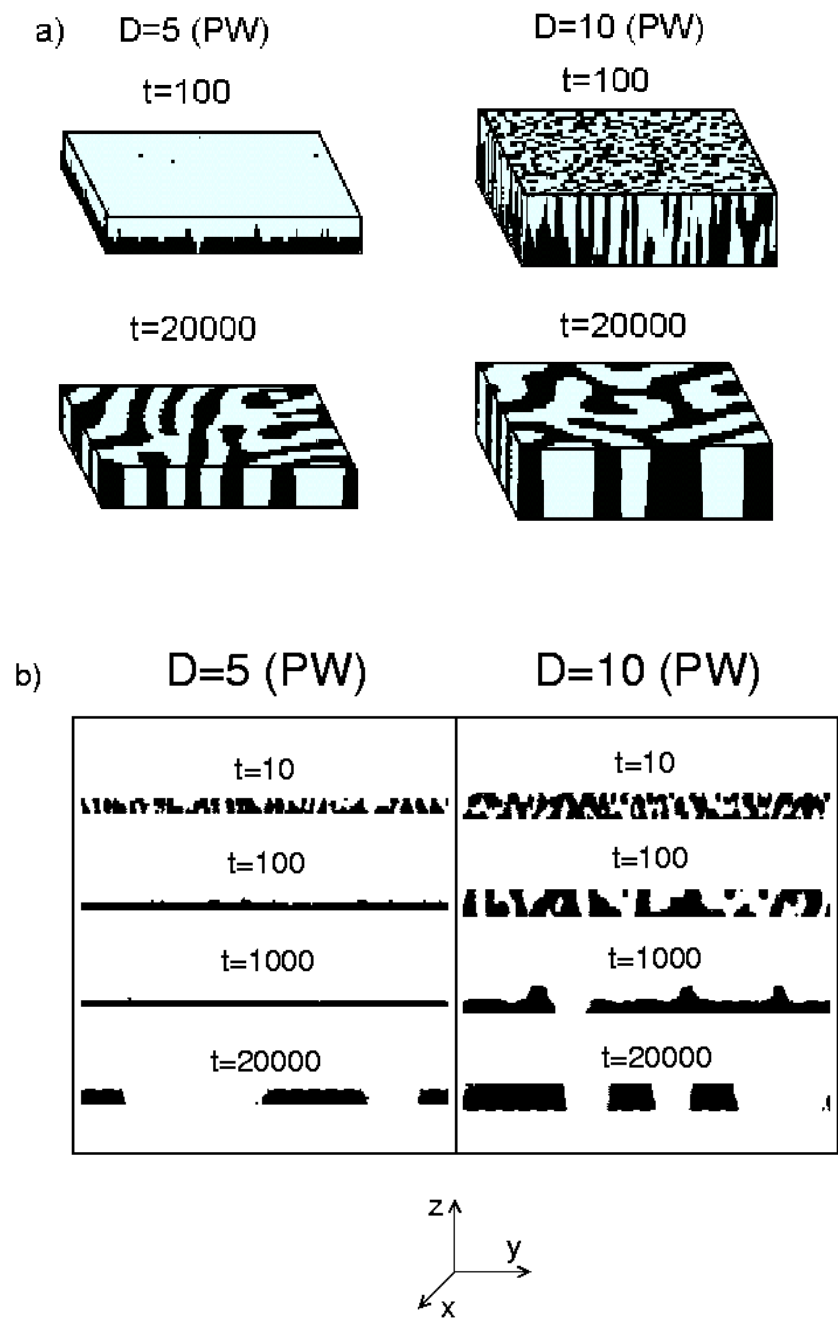


FIG. 11: Analogous to Fig. 2, but for an antisymmetric film with a PW morphology.

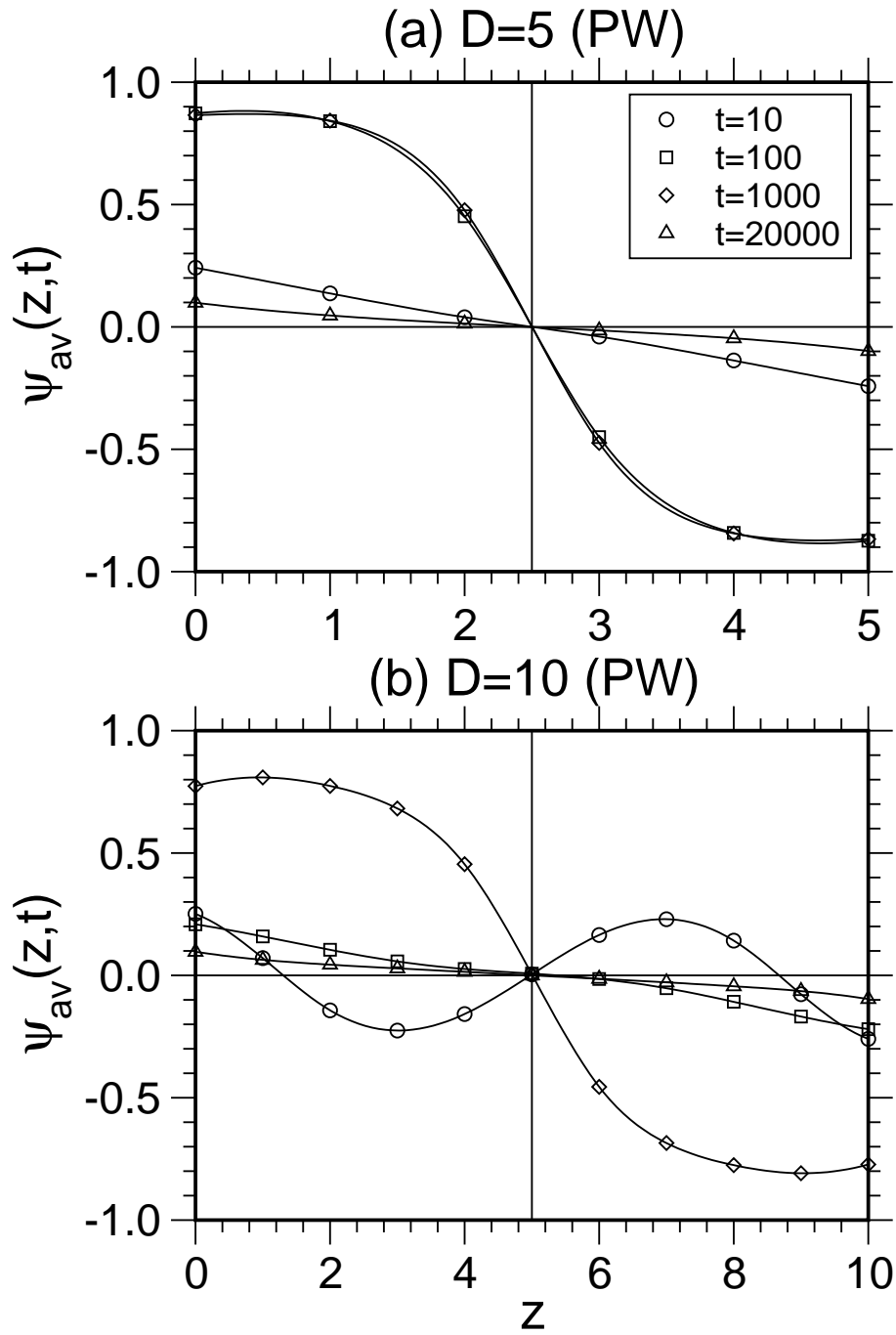
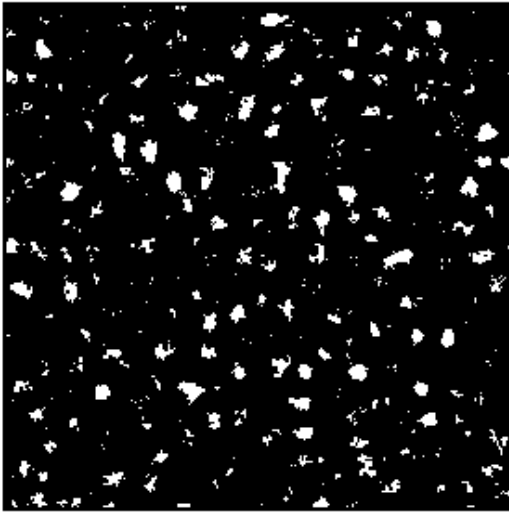


FIG. 12: Laterally averaged profiles for the evolution depicted in Fig. 11 at the dimensionless times  $t = 10, 100, 1000, 20000$ , for (a)  $D = 5$ , and (b)  $D = 10$ .



(a)  $D=5$  (PW)

$t=100$

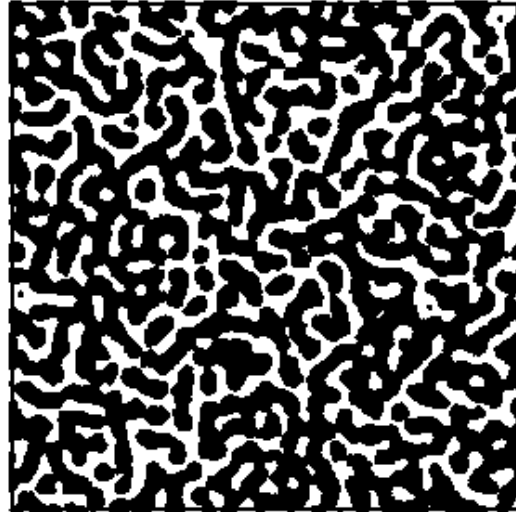


↓  
 $t=20000$



(b)  $D=10$  (PW)

$t=100$



↓  
 $t=20000$



FIG. 13: Cross-sections of the evolution snapshots in Fig. 11(a). The cross-sections are taken parallel to the surfaces at (a)  $z = 2$  for  $D = 5$ , and (b)  $z = 5$  for  $D = 10$ .

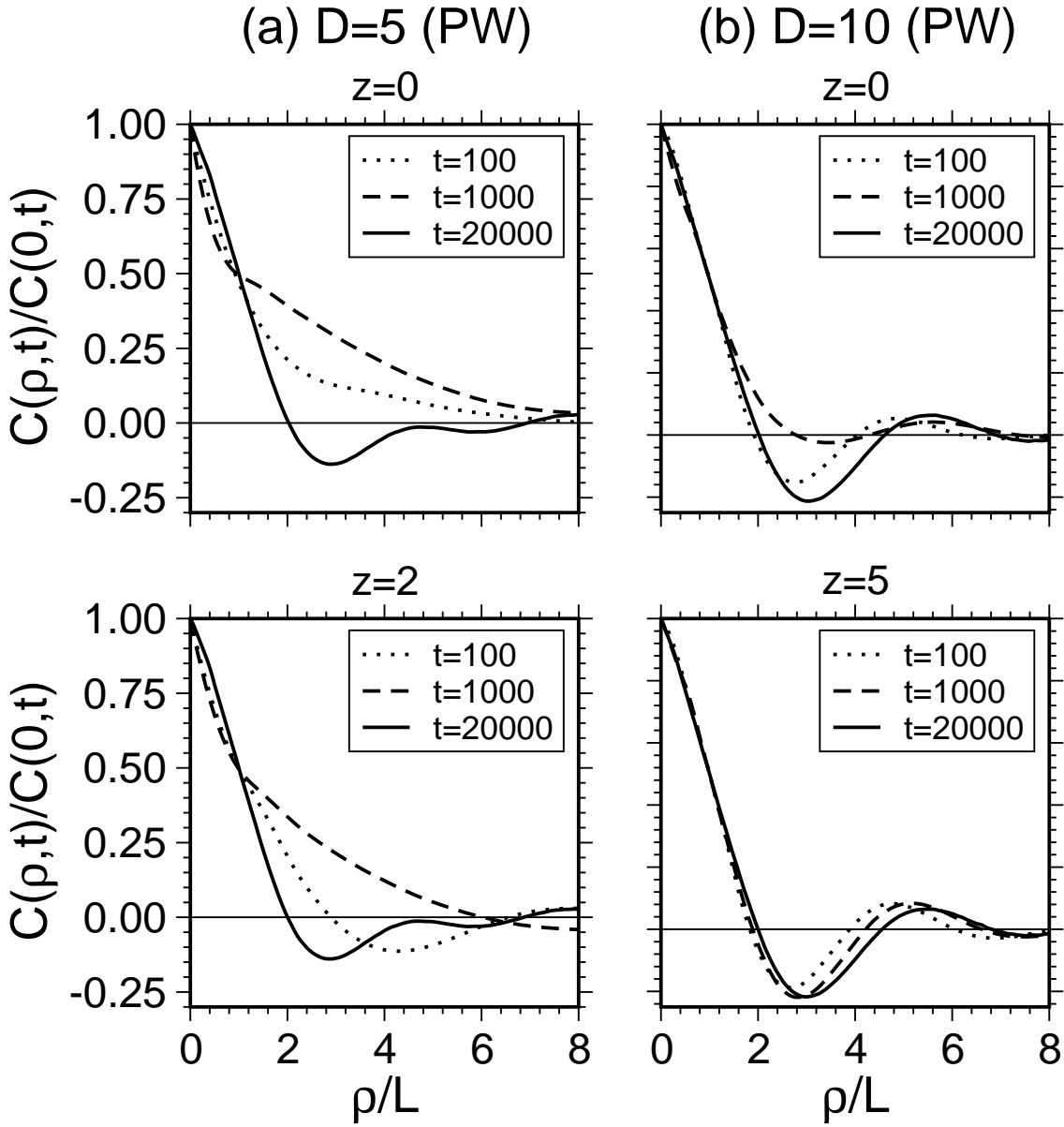


FIG. 14: Scaling plot of layer-wise correlation functions for the evolution depicted in Fig. 11. We plot  $C(\rho, t)/C(0, t)$  vs.  $\rho/L$  for  $t = 100, 1000, 20000$ . We present data for (a)  $D = 5$  at  $z = 0$  (wall) and  $z = 2$  (center); and (b)  $D = 10$  at  $z = 0$  (wall) and  $z = 5$  (center).

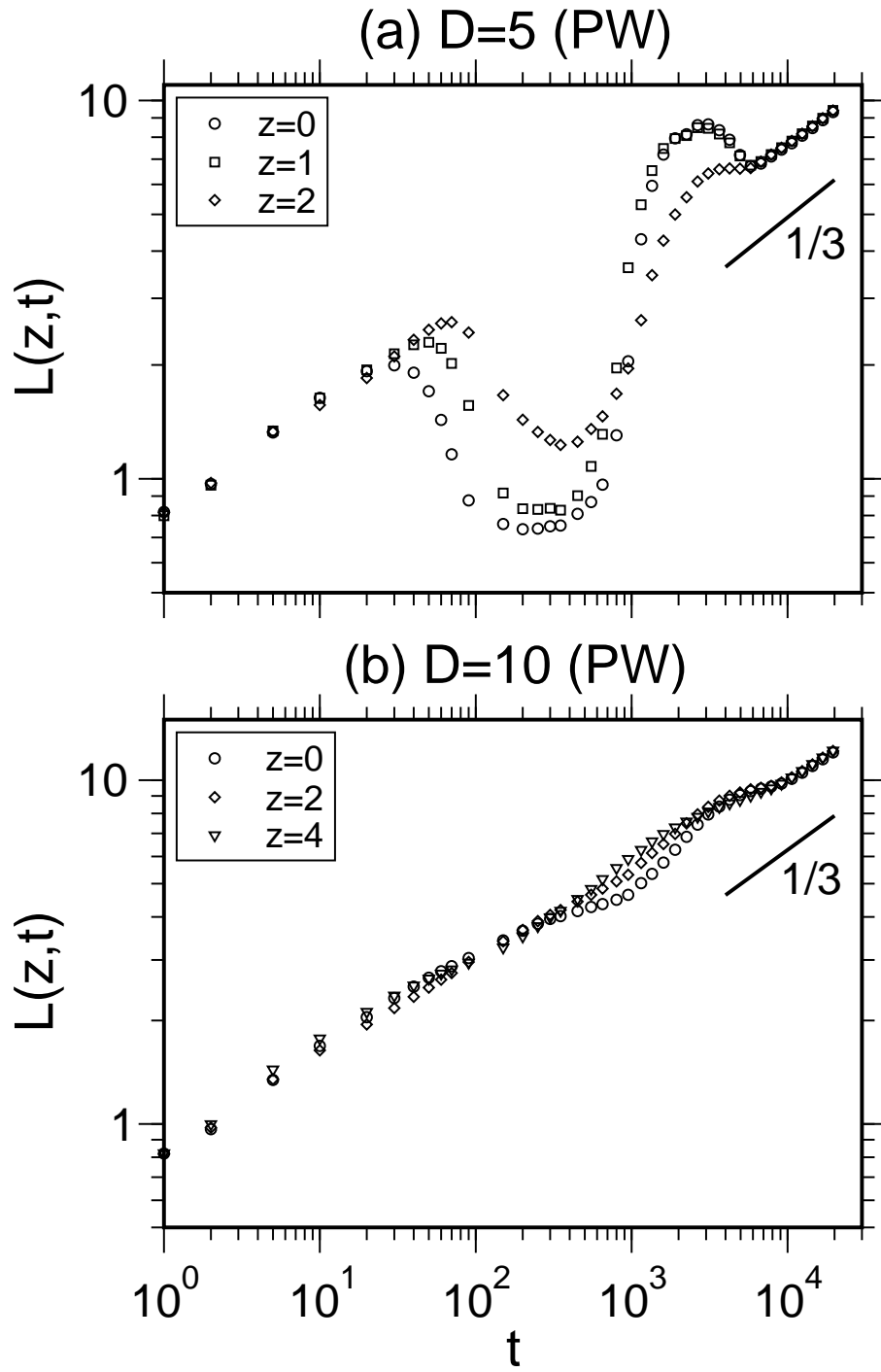


FIG. 15: Time-dependence of the layer-wise length scale for the evolution depicted in Fig. 11. We plot  $L(z,t)$  vs.  $t$  on a log-log scale for various values of  $z$  and (a)  $D = 5$ , and (b)  $D = 10$ .

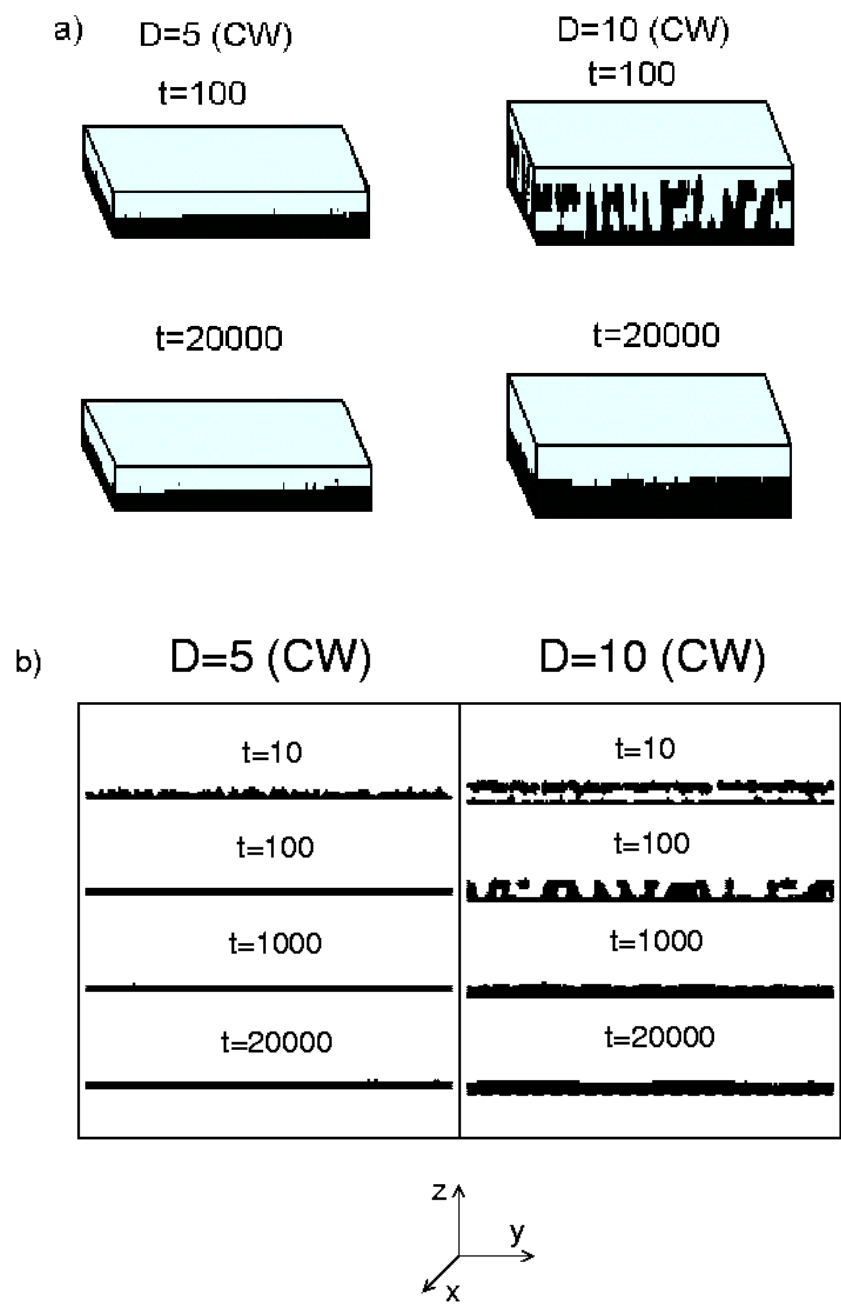


FIG. 16: Analogous to Fig. 2, but for an antisymmetric film with a CW morphology.

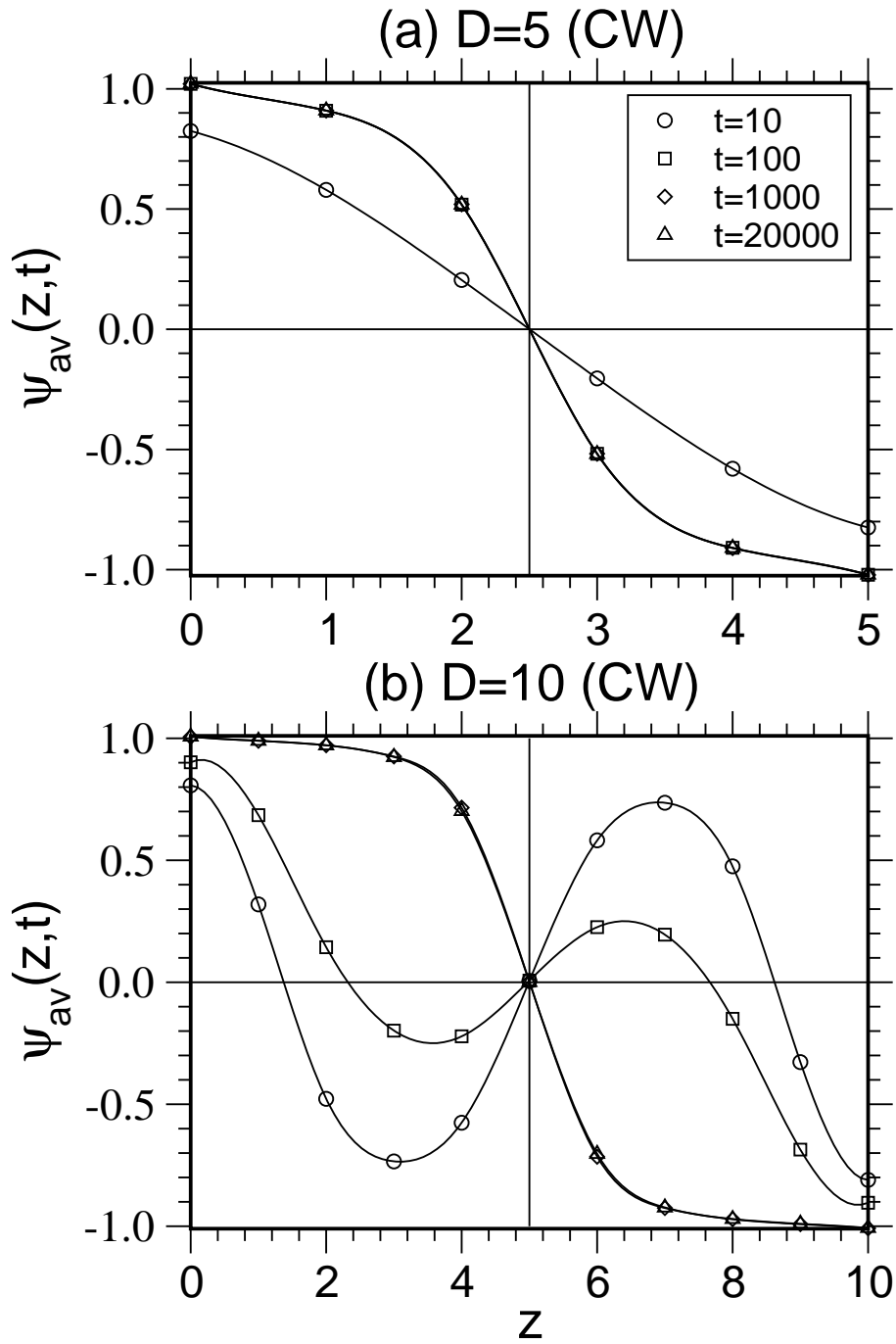
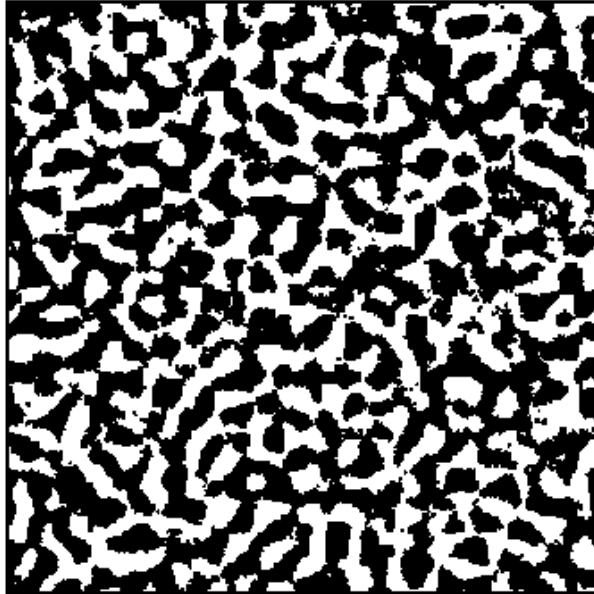


FIG. 17: Laterally averaged profiles for the evolution depicted in Fig. 16, for (a)  $D = 5$ , and (b)  $D = 10$ .

$D=10$  (CW)

$t=100$



$t=20000$

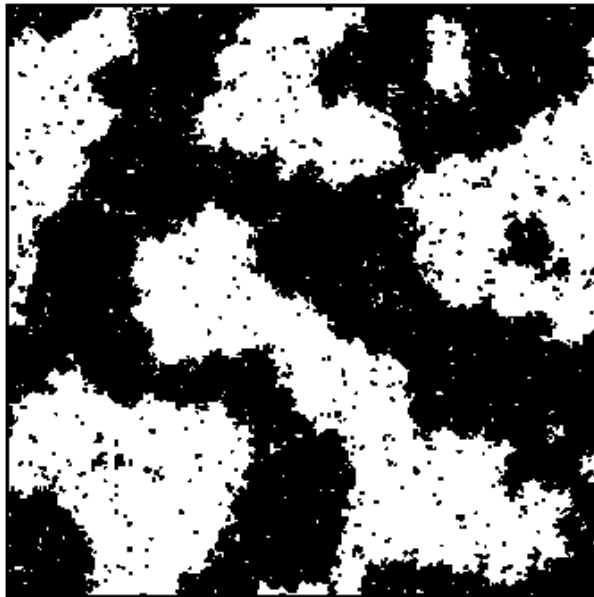


FIG. 18: Cross-sections of the evolution snapshots for  $D = 10$  in Fig. 16(a). The cross-section is taken parallel to the surfaces at  $z = 5$ .

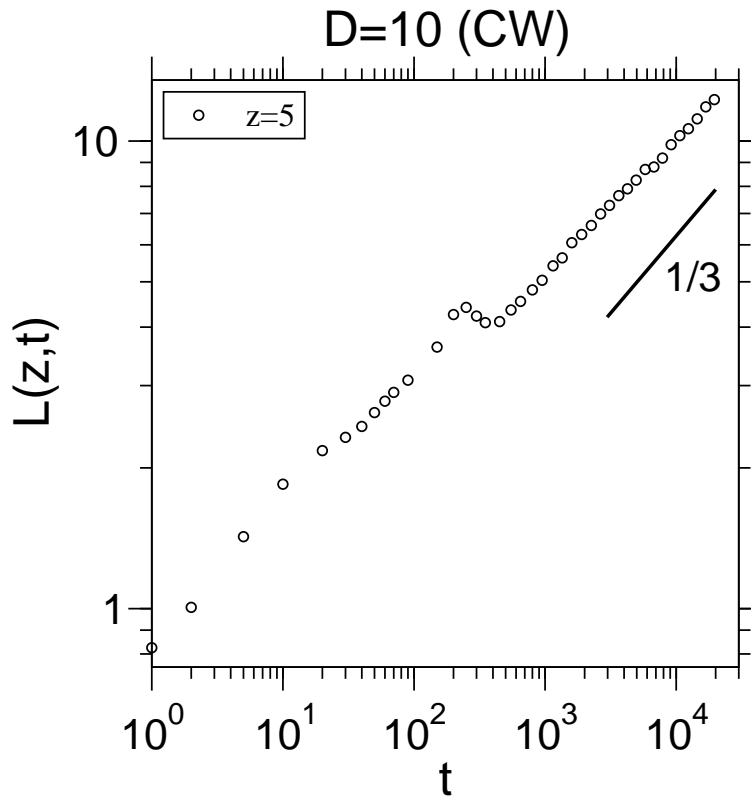


FIG. 19: Time-dependence of the layer-wise length scale for the  $D = 10$  evolution depicted in Fig. 16. We plot  $L(z, t)$  vs.  $t$  on a log-log scale for  $z = 5$ .